Neural representations of haptic object size in the human brain revealed by multivoxel fMRI patterns

Perini, Francesca; Powell, Thomas; Watt, Simon; Downing, Paul

Journal of Neurophysiology

DOI:
10.1152/jn.00160.2020

Published: 01/07/2020

Peer reviewed version

Neural representations of haptic object size in the human brain revealed by multivoxel fMRI patterns

Francesca Perini[1], Thomas Powell[2], Simon Watt[3] and Paul E. Downing[3*]

1. Centre for Sleep and Cognition, Yong Loo Lin School of Medicine, National University of Singapore, Singapore, 117597

2. Netherlands Applied Science Organisation (TNO), Oude Waalsdorperweg 63, Den Haag, Netherlands

3. School of Psychology, Bangor University, Bangor, UK

* For correspondence: p.downing@bangor.ac.uk

Abstract

The brain must interpret sensory input from diverse receptor systems to estimate object properties. Much has been learned about the brain mechanisms behind these processes in vision, while our understanding of haptic perception remains less clear. Here we examined haptic judgments of object size, which require integrating multiple cutaneous and proprioceptive afferent signals, as a model problem. To identify candidate human brain regions that support this process, participants (N=16) in an event-related fMRI experiment grasped objects to categorise them as one of four sizes. Object sizes were calibrated psychophysically to be equally distinct for each participant. We applied representational similarity logic to whole-brain, multi-voxel searchlight analyses to identify brain regions that exhibit size-relevant voxelwise activity patterns. Of particular interest was to identify regions for which more similar sizes produce more similar patterns of activity, which constitutes evidence of a metric size code. Regions of the intraparietal sulcus and the lateral prefrontal cortex met this criterion, both within-hands and across-hands. We suggest that these regions compute representations of haptic size that abstract over the specific peripheral afferent signals generated in a grasp. Results of a matched visual size task, performed by the same participants and analysed in the same fashion, identified similar regions, indicating that these representations may be partly modality-general. We consider these results with respect to perspectives on magnitude estimation in general and to computational views on perceptual signal integration.

New & Noteworthy

Our understanding of the neural basis of haptics (perceiving the world through touch) remains incomplete. We used fMRI to study human haptic judgments of object size, which require integrating multiple afferent signals. Multivoxel pattern analyses identified intraparietal and prefrontal regions that encode size haptically in a metric and hand-invariant fashion. Effector-independent haptic size estimates are useful on their own, and in combination with other sensory estimates, for a variety of perceptual and motor tasks.

Introduction

The brain must transform the implicit information carried in a constant flow of sensory input into explicit information about the world around us. Decades of visual neuroscience have revealed much about how this is achieved through cascades of activity in hierarchically organised maps of the visual world (Di Carlo et al., 2012; Kravitz et al., 2013). We know less, however, about the brain systems that support *haptics*: the discovery of object properties through active touch (Hsiao, 2008; Yau et al., 2015). The aim of the present study is to learn more about the human neural systems underpinning haptic object representation. We focus on understanding a model problem—haptic perception of object size—that has several useful properties: it allows the fine control of experimental parameters; there is existing psychophysical and neurophysiological evidence on how it is achieved; and it relates to important problems in multimodal integration and in tool use.

The perceptual foundations of the haptic system are in cutaneous afferents arising from nerves under the skin's surface, and proprioceptive signals arising from receptors embedded in muscles, tendons and joints (Delhaye et al., 2018; Lederman and Klatzky, 2009). Cutaneous receptors report on properties such as vibration, surface texture, pattern, local edges, and temperature (Jones and Lederman, 2006), whilst proprioceptive signals convey finger and limb position or posture (Taylor, 2009). A key challenge for haptic perception is that multiple tactile "views" of an object (arising from different sources and different parts of the hand and fingers) must be integrated with knowledge of hand and digit positions to achieve a representation that can be compared to stored knowledge for object localisation, recognition, and action (Heed et al., 2015; Hsiao, 2008; Klatzky et al., 1985; Yau et al., 2015).

On the face of it, haptic size can be conveyed by the proprioceptive signals and skin-stretch receptors that signal the separation of the grasping digits (Edin and Johansson, 1995; Lederman and Klatzky, 2009). Digit separation does not reflect object size entirely reliably, however, because the pulpar surfaces of the digits are compressed by different amounts depending on the grip force applied, and we frequently grasp compliant objects (Bruno and Bertamini, 2010; Garrett et al.,1996; Reed et al., 1990; Terada et al., 2006). Thus, different digit separations can result from feeling the same object. Berryman and colleagues (2006) showed that human haptic size estimates are

largely unaffected by variations in either grip force or object compliance, suggesting that tactile signals—about the deformation of digit tips and material properties of object surfaces—are used to compensate for these changes in digit separation, yielding robust estimates of haptic object size. Thus, haptic estimates of object size are a good example of how information from multiple sensory signals must be integrated to provide useful information about an object's properties.

Much of our understanding about how afferent haptic signals are processed and integrated in the brain comes from single-unit recording and lesion studies in non-human primates (Hsiao, 2008; Sathian, 2016). These studies indicate a hierarchy of increasingly complex and integrated response properties (Yau et al., 2015). Initially, distinct sources of haptic information are thought to be segregated: area 3a neurons are mainly driven by proprioceptive signals, whereas in area 3b, cutaneous stimulation is more effective. Several lines of evidence suggest that the neurons of areas 1 and 2 within primary somatosensory cortex (SI) occupy a higher level in the hierarchy: they receive inputs from 3b as well as from the thalamus; they include receptive fields that span more than one digit; and area 2 neurons in particular respond both to cutaneous and proprioceptive stimulation, such that sensitivity to cutaneous inputs is modulated by hand posture. Outputs of SI extend via a putative "ventral stream" to area SII, and dorsally to the intraparietal sulcus and other regions (Sathian, 2016). Relative to SI neurons, SII neurons tend to have larger receptive fields; further, they can span both the contra-and ipsi-lateral hands, and some respond to tactile object features such as edge orientation in a position-invariant manner. In these respects, SII may provide the kinds of integrated representations that would be key for establishing the size of a grasped object. Collectively, such findings describe a scheme in which cortical regions that are closest (in terms of connectivity) to the afferent input have relatively simple, local responses, with further stages of cortical processing performing a broader synthesis of more complex features as well as integrating of multiple types of input. (However, a simplistic hierarchical view is challenged by evidence for rapid and non-linear interactions between cutaneous and proprioceptive signals right through to areas 3a and 3b, in the presumed lower levels of the hierarchy; Kim et al., 2015).

Neuroimaging studies have identified human brain regions that respond to a variety of object properties and tasks in the tactile modality (Bodegård et al., 2001; Deibert et al., 1999; Lederman et al., 2001; Miquee et al., 2008; Peltier et al., 2007; Reed et al., 2004;

Savini et al., 2010; Simoes-Franklin et al., 2011; Stoeckel et al., 2003; Stoesz et al., 2003). Relatively few of these have focused specifically on object size. An early PET study, for example (O'Sullivan et al., 1994) compared somatosensory discrimination of texture and object length, finding relatively increased activity for the latter task in broad lateral parietal regions.

Explorations of object size have tended to be more common in vision, as part of an effort to understand the contribution of size representations to object-directed grasps. For example, in a study of the size-weight illusion, Chouinard et al. (2009) used fMRI repetition suppression to identify regions that code for the size, weight and density of lifted objects. Regions of contralateral S1, anterior intraparietal sulcus, superior parietal lobule, and the fusiform gyrus showed activity relating to stimulus size. However, these activations may be attributable to visual or haptic size (or both). Similarly, Monaco et al. (2015; see also Fabbri et al., 2016) used a repetition suppression approach to distinguish coding of intrinsic object properties (e.g. size) from extrinsic properties (e.g. location). Repetition suppression for object size was found in the anterior intraparietal sulcus; but because the objects were visible to the participants, it is not possible to distinguish encoding of visual from haptic size from these results.

If, in an action context, object size is generally available from vision, then to what ends might the brain compute a haptic-specific estimate of size? Of course, there are many situations when vision is not available (finding the right coin in one's pocket, fixing out-of-vision parts of a car engine). But haptic estimates routinely contribute to object perception even when they provide redundant information to vision. In this situation the brain does not rely preferentially on one sense, but instead integrates visual and haptic estimates, such that both contribute to the eventual estimate (indeed, haptics can be the more informative signal, and thus given more 'weight'; Ernst and Banks, 2002; Gepshtein and Banks, 2003). Specifically, there is evidence that the brain exploits the statistical redundancy inherent in multiple signals to produce an integrated estimate that is more precise than is possible from either signal alone (Clark and Yuille 1990; Ernst and Banks, 2002; Ghahramani et al., 1997; Landy et al., 1995). Haptic-specific size estimates are likely a necessary computational step towards such integrated estimates.

To better understand where and how haptic object size is represented in the human brain, we took a *representational similarity* approach to fMRI design and analysis

(Kriegeskorte et al., 2008). The aim was to identify brain regions on the basis of their representational structure rather than measuring gross mean changes in activity level. The approach, a form of multivoxel pattern analysis (MVPA; Haxby et al., 2001; Haynes et al., 2006; Norman et al., 2006), centres on measuring the similarity between local patterns of brain activity and specific hypothesised properties of the representation of a task or stimulus. Here, these analyses were performed on fMRI data from a simple task in which participants grasped unseen cuboid objects of different sizes with either the left or right hand, and then reported which of several object sizes was presented. In order to select object sizes that were equally perceptually distinct, we measured each participant's size-discrimination thresholds using a psychophysical procedure prior to the fMRI study.

For any given brain region, we can use the representational similarity logic to ask to what extent the patterns of activity evoked by an object of a given size are 1) *reliable* across scanning runs, and 2) *distinct* for different sizes (cf. Haxby et al., 2001). A region exhibiting these properties could be considered to encode one or more aspects of haptic size. A further key expectation is that 3) *more similar sizes should evoke more similar patterns of activity.* This is a representational property that we would expect of a metric size representation. Further still, we can seek regions that exhibit this metric scaling of responses, and also do so 4) *across hands*, such that the pattern of responses evoked by a given size is similar whether the object was grasped by the left or right hand. A region fitting the latter of these criteria in particular could be said to represent haptic size in a metric way that is abstract over the peripheral mechanics of making specific movements with a specific hand.

Finally, we can compare the brain responses in a haptic size task to those generated in a comparable visual size task (with hemifield of presentation standing in for left vs right hand). This final step allows us to distinguish size representations that relate to haptics, specifically, from those engaged by more abstract or amodal size encoding. In sum, with this experimental logic, we are able to go beyond identifying brain regions that are simply engaged in some way by a haptic size judgment, to distinguish regions that capture more or less abstracted, and metric, representations of object size.

We conducted the multivoxel pattern analyses described above using a whole-brain volumetric "searchlight" approach (Etzel et al., 2013; Kriegeskorte et al., 2006). This

approach allows us to identify regions with haptic size representations anywhere in the brain, without committing *a priori* to regions of interest. An important caveat to the multivoxel approach is that its spatial resolution in limited, relative to univariate approaches, by the need to assess patterns over a local neighbourhood of multiple voxels.

In sum, we sought to identify regions of the human brain that may contribute, at varying levels of abstraction and specificity, to making judgments about object size from haptic information.

Methods

Participants. Sixteen right-handed participants (13 female; mean age 27 years, SD = 7.0, range 20-40) were recruited from the Bangor University community. All participants had normal or corrected-to-normal vision. Participants satisfied all safety requirements in volunteer screening, and gave written informed consent. The experimental procedures were approved by the Ethics Committee of the School of Psychology at Bangor University. Participation was compensated at £40 for the whole study.

Design overview. A behavioral study was conducted first, with two aims. First, we sought to confirm that haptic size sensitivity was similar for the left and right hands, so that brain activity elicited by both kinds of grasp would be directly comparable. Second, we sought to identify for the fMRI experiment four unique stimulus sizes for each participant that were equally distinct subjectively. Our aim here was to 'linearize' the representational similarity space, such that patterns of activity for different object sizes would differ by similar amounts. Thus, the similarity space describing the representations of these different object sizes should be directly comparable across different object sizes, and across participants.

The same participants returned for two separate fMRI imaging sessions—one to perform the haptic task and the other to perform the visual task. In the haptic session, participants grasped different sized blocks and performed a size classification task. In the visual session, they judged the size of visual stimuli presented on the screen. Half of the participants performed the haptic session first, and the other half the visual session first.

Insert Figure 1 about here.

Out-of-scanner haptic size-discrimination task. Each participant completed a ~3 hour psychophysical experiment to determine individual sensitivity to haptic size for grasps by each hand (**Fig. 1**). We created rigid haptic "objects" of different sizes using a custom computer-controlled device that altered the separation of two rigid planes (each 100 mm wide) by moving them along a track using high-precision stepper motors (Fig 1a). The position of each plane was controlled by a separate motor, in increments of ~0.1 mm. The minimum possible object size was 6.7 mm and the maximum possible object size exceeded the hand opening.

Size-discrimination was assessed using a two-interval, forced-choice task. On each trial, participants grasped two consecutive stimuli, either with only the left or only the right hand, and reported which one was larger (Fig 1c). The stimuli and hand were out of view of the participant, under a screen (Fig 1b). Participants wore earplugs to minimise distractions from the sounds made by the stimulus device, and to minimise the likelihood of them attempting to use these sounds as a cue to changes in object size. The device was also programmed to make a short series of random movements before stopping at each size, so that sound was not informative about changes in size. A short auditory tone, audible through the earplugs, indicated when to grasp each stimulus. The overall position of the object was also jittered by moving both planes in the same direction by a small random amount (up to 10 mm), to prevent the task being completed by monitoring the position of one digit only. We measured just-noticeable differences (JNDs) in size for five standard sizes: 10, 20, 30, 40 and 50 mm. Order of the standard and comparison stimuli was chosen at random on each trial. For the four largest standard sizes the comparison sizes were controlled using two adaptive staircase procedures (1-up, 2-down, and 2-up, 1-down), which concentrated trials in the most informative regions for determining the parameters of the psychometric function. It was not possible to use a 2-up, 1-down staircase for the 10 mm standard because it would likely result in comparison sizes smaller than our device could present (and possibly smaller than zero). For this standard size we therefore repeated the 1-up, 2-down staircase. The staircases changed with an initial step of 8 mm, which was halved after each of the first three reversals (i.e. steps of 4, 2, then 1 mm). Staircases terminated after 12 reversals. Staircases for the different object sizes were randomly interleaved, and blocked by reversal rule. One repetition of each staircase was performed for each hand, and object size (i.e. two staircases per psychometric function). Haptic size JNDs were defined as the standard deviation of the best-fitting cumulative Gaussian to the size-discrimination data, using a maximum-likelihood criterion (Fig 1d).

To specify each participant's object sizes for the fMRI experiment, we first determined JNDs for each participant for each hand at each object size. We then characterized the continuous relationship between these JNDs and object size for each participant's left- and right-hand by fitting their JND data with a second-order polynomial (Fig 1e). These fitted curves were then used to establish a candidate set of four object sizes for the fMRI experiment that should be equally perceptually distinct (Fig 1e). Sizes 2 and 3

were specified with respect to an arbitrary 30 mm 'baseline', by subtracting and adding, respectively, the participant's JND at 30 mm (derived from the fitted curve). Size 1 was calculated by subtracting 2 JNDs at size 2 from size 2. Similarly, size 4 was calculated as size 3 plus 2 JNDs at size 3 (Fig 1e). Thus, all four sizes were spaced 2 JNDs apart. The resulting set of sizes were similar across the two hands, with mean differences at each size of < 0.5 mm, and a non-significant hand x object size interaction ($F(3,13) = 1.1$, $p = 0.386$). We therefore averaged the object sizes across the two hands yielding four object sizes for use in the fMRI experiment, on a participant-by-participant basis. These sizes were, on average across participants, 12.8 mm (SD= 5.31 mm); 23.5 mm (2.26); 36.5 mm (2.26); 51.6 mm (8.22).

Insert Figure 2 about here.

Haptic fMRI task. Participants grasped wooden blocks of the four different sizes determined in the out-of-scanner task. (Apart from the difference in the grasped dimension, the stimuli were otherwise identical.) These were presented to the participant via a sliding presentation tray that was moved by an experimenter who stood alongside the scanner **(Fig. 2, top)**. The positioning of stimuli on the presentation tray was randomised between participants. Participants wore earphones for hearing protection and to receive auditory cues about when to perform grasping actions. A monitor mounted at the back of the scanner bore, and visible to the participant through an angled, coil-mounted mirror, enabled us to convey task instructions and response options to the participant. A custom MR-compatible foot pedal (built around a Current Designs fiber-optic response pad) was mounted at the end of the scanner bed, allowing participants to respond by foot press. A data projector was mounted in the control room so that it projected into the scanner chamber, with the image visible to the experimenter but not to the participant. This was used to instruct the experimenter about the next stimulus size to place. All cues were presented and participant responses collected using Matlab (Matlab R2010b, Mathworks) with PsychToolbox (Brainard, 1997; Kleiner et al., 2007; Pelli, 1997).

Participants lay supine in the scanner and grasped the stimuli (which they could not see) by performing a precision grip using the thumb and index finger of the left or right hand. The sequence of a single trial is illustrated in **Fig. 2 (bottom)**. Each trial started with a visually-presented cue word ("left" or "right") lasting 200 ms, to indicate which

hand should be used. This was followed by a brief tone informing the participant to make the movement. Participants were trained to complete the grasping movement within 1.4 seconds. Between trials, participants rested their thumb and forefinger on elevated pads adjacent to the stimuli, while the experimenter moved the presentation tray to the next stimulus. This starting position was designed to minimize the movement required in the scanner, and to minimize participants' uncertainty about where the unseen object was positioned. Participants were asked to maintain central fixation throughout the study.

Before the scanning session, participants were told that the objects they would grasp would be one of four sizes – labelled "A", "B", "C", and "D" from smallest to largest. These alphabetical categorical labels were used instead of numbers in order to weaken any influence of automatic links between response category and object size (cf. Moretto and di Pellegrino, 2008). In each trial, after the participant grasped the stimulus, these four letters were presented sequentially on the screen, each for 780 ms. The letter that was presented first was selected randomly and then the subsequent letters were cycled (in a random order determined separately for each run) until the participant responded or until the trial duration expired. To avoid contaminating the neural response produced by manual object grasping with response-related movements, participants used their right foot to press the foot pedal when the letter on the screen corresponded to the size of the stimulus they had just grasped. After the foot button press, the letter turned from white to green to indicate a correct response, or to red to indicate an incorrect response. The total duration of each trial was fixed at 6.0 s.

Participants' hand movements were video recorded to check that they were correctly performing the task. In addition, the experimenter in the scanner suite was able to monitor for errors. These were not common, and were mainly due to difficulty in pressing the foot device on time, as reported by participants on debriefing. For this reason, all trials have been included in the analysis of the fMRI data.

Visual fMRI task. Participants were instructed to keep their eyes on a central fixation dot for the duration of each trial. Visual stimuli were presented on the back-projection screen. These were white rectangles presented on a black background, either to the left or right of the central fixation point. The on-screen size of the visual stimuli corresponded exactly to the physical size of the haptic stimuli, determined separately

for each participant. The word “left” or “right” appeared onscreen at the start of each trial as in the haptic task, but here it indicated on which side the stimulus would appear. The event timings of trials were as in the haptic experiment, and participants responded in the same manner.

Design. Stimulus size and laterality (grasping hand in the haptic session; visual location in the visual session) were varied over an event-related design. In addition to the eight conditions created by a factorial combination of size (4 levels) and hand (2 levels), a ninth null condition, consisting of 6 s of fixation only, was included. These null trials served as a baseline and also had the effect of increasing the amount of temporal jitter amongst task trials. Trial sequences of 82 trials were generated with custom code such that each of the 9 conditions was preceded equally often by each condition. The first trial of each 82-trial sequence served only to provide a context for the following one (so that all trials had a balanced “history”), and was discarded from the analysis. These trial sequences were then split in half over two experimental runs, with the final trial of the first half being repeated at the start of the second run. Each participant was tested on four such pairs of runs, resulting in 8 total runs and 36 trials per condition. (For two participants only 6 runs were acquired in the haptic task). Each run was bookended with 12 s of fixation, resulting in runs of 4:30.

These functional scans were preceded by an anatomical scan, during which the participant performed a training run of the task (data discarded).

Scanning Parameters. Structural and functional data were collected using a 3T Philips Achieva MRI scanner, equipped with a SENSE parallel head coil (Philips, Best, Netherlands). Functional data were collected with T2*-weighted scans using an echo planar (EPI) sequence. 135 volumes were collected in each run, 1080 per subject per session in total. 28 off-axial slices were acquired with a 240 mm field of view (FOV), 96 x 96 matrix size, with a slice thickness of 3 mm and 2.5 x 2.5 mm in-plane resolution. Slices were acquired in interleaved order with no interslice gap. An echo time (TE) of 35 ms was used with a 2000 ms repetition time (TR) and a 90^{o} flip angle. Slice positioning began at the dorsal apex of the brain, covering all dorsal frontal and parietal regions and excluding ventral temporal and occipital regions to varying degrees depending on brain size (see additional online materials).

A structural T1-weighted scan was taken for anatomical localisation for each participant, using the following parameters: FOV = 256 mm, 256 x 256 matrix, slice thickness = 1 mm; voxel dimensions = 1x1 mm in-plane; TR = 16 ms; TE = 3 ms; flip angle = 8°.

Image analysis. Data were preprocessed and analysed using SPM12 (http://www.fil.ion.ucl.ac.uk/spm/) and custom Matlab scripts. Preprocessing steps included realignment; coregistration of anatomical to functional image space; and transformation of both image sets to MNI space. Multiple regression analyses conducted separately on unsmoothed data from each scanning run, for each participant individually, formed the basis of the MVPA analysis. The predictors in these models consisted of one regressor for each combination of object size (four levels) with laterality (haptic session: left or right hand; visual session: left or right retinal location). A further regressor captured foot responses. These regressors were constructed by convolution of a hypothesised neural event (starting at 800 ms after the cue to act was given, and lasting for 400 ms) with a canonical hemodynamic response function. Regressors of no interest derived from the realignment results were also included in the analyses.

Insert Figure 3 about here.

Multivoxel pattern analysis. Hypothetical neural similarity matrices (**Fig. 3**) capture different ways that distributed patterns of brain activity may relate systematically to object size. They describe predictions for the similarity relationships amongst activity patterns in a given area, across pairs of scanning runs. In each matrix, higher values in a cell express the prediction of a relatively higher positive correlation between the activity patterns evoked by the two conditions in question, across two independent runs of the experiment. In turn, lower values express a prediction of relatively low similarity in patterns of neural activity. These matrices apply to both the haptic and visual tasks, but in our description here we focus on the haptic case of main interest.

The first matrix is similar in logic to the approach of Haxby et al. (2001). It expresses the prediction that the response patterns to a given object size, grasped with a given hand, should be a) reliable, in the sense of being similar across scanning runs, and b) distinct, in the sense of being more similar than the patterns evoked by any different combination of object size and hand.

The second matrix captures the prediction that grasping two objects of relatively similar sizes with the same hand will produce similar patterns of brain activity, relative to objects of more dissimilar sizes. Such a representation would be metrically related to the size of objects, without necessarily responding differentially on average to different sizes. As such it would be a good candidate for a region that is functionally relevant for haptic grasping tasks. In this matrix, the cross-hand cells are empty (zero). Hence the similarities of patterns that are evoked across two runs by grasps with different hands do not contribute to this analysis.

The third matrix mirrors the second one to examine the cross-hand case. That is, it expresses the prediction that grasping objects of similar sizes will produce similar patterns of brain activity across different hands. A region exhibiting this property of metric cross-hand representations would be consistent with a relatively abstract haptic representation of size, independent of at least the most peripheral sensorimotor processes related performing a grasp with a specific hand.

Because the second and third matrices are orthogonal to each other, any given region could in principle express either, both, or neither of the predicted similarity patterns. However, it seems likely that a region that is sensitive to haptic size across hands (matrix 3) would also be so within hands (matrix 2), but this is not necessarily so *vice versa*.

We also include an analysis based on a fourth matrix that is simply the sum of matrices 2 and 3. While this does not test distinct predictions to those matrices, it has the advantage of increased power and sensitivity in that it reflects all of the collected data, rather than half as for matrices 2 and 3. For this reason, we used results from this matrix to compare the haptic results with those from the visual size task.

Insert Figure 4 about here.

Whole-brain searchlight. fMRI data were analysed with a multivoxel "searchlight" technique (Kriegeskorte et al., 2006). An approximately spherical searchlight of 5 voxels in diameter in resampled space (voxels of 3 mm x 2.5 mm x 2.5 mm; 25 voxels in total) was centred at each unique location in the scanned brain volume. This searchlight volume was selected to balance spatial precision with sensitivity to locally-distributed pattern information. At each location, a vector of 25 beta values for each of the eight

412 experimental conditions was extracted (combination of four object sizes x hand
413 laterality; null events excluded). These patterns of beta values were the raw materials
414 for subsequent steps that tested for robust patterns of activity corresponding to the
415 prediction matrices. These steps are outlined in **Fig. 4**.

416 For each participant, each unique pairing of the 8 experimental runs was assessed (28
417 pairs of runs). This approach was motivated by previous findings that for multivoxel
418 analyses it can be preferable to have relatively more (albeit noisier) estimates of activity
419 patterns relative to fewer, more stable ones (e.g. as in a split-half correlation; cf.
420 Coutanche and Thompson-Schill, 2012). At each location of the searchlight, the
421 patterns of beta values were correlated for all of the conditions across a given pair of
422 runs, resulting in an 8 [conditions] x 8 [conditions] correlation matrix. Each correlation
423 matrix was multiplied, element-wise, by each of the prediction matrices shown in **Fig. 3**.
424 The mean of the resulting 8x8 matrix was then recorded in a results map at the centre
425 of the searchlight location. (Conceptually, this is similar to a contrast analysis, e.g. in a
426 one-way ANOVA of a design with multiple levels, in which a specific hypothesis about
427 relative differences between conditions is expressed by a series of contrast weights that
428 sum to zero.) The prediction matrices were normalised to have a mean value, and a
429 sum, of zero (Table 1). In this way, the values of the results map were positive to the
430 extent that the observed and predicted patterns of similarity were found at that location,
431 with a null distribution centred on zero. The 28 results maps for each participant were
432 Fisher transformed to improve normality, then averaged.

433 Following this procedure, each participant had eight results maps, one for each of the
434 four prediction matrices, separately for the haptic and visual tasks. To improve cross-
435 participant alignment and to account for the smoothness of the underlying searchlight
436 analysis, each results map was spatially smoothed (4x4x4 mm FWHM Gaussian
437 kernel). These maps were then subjected to second-level random-effects analyses, as
438 reported below. Further, to directly compare between the visual and haptic tasks with
439 the fourth prediction matrix, we subtracted the maps for the two modalities at the
440 individual level, and these difference maps were entered into a second-level random-
441 effects analysis.

Results

Analyses of accuracy on the in-scanner data, tested with an ANOVA with modality (visual/haptic), laterality (left/right), and object size (four sizes) as factors, did not reveal any significant interactions, all $F < 2.6$, $p > 0.09$. Performance was better on the visual (92.5%; SD = 3.96) than on the haptic (89.6%, SD = 4.1) task, $F(1,15) = 6.8$, $p = 0.02$. There was no significant main effect of laterality, $F(1,15) = 0.67$, $p = 0.43$. Participants were better overall at judging the smaller than the larger sizes (size A: 95.3%, SD = 2.0; size B: 92.5%, SD = 4.8; size C: 88.4%, SD = 6.4; size D: 88.1%, SD = 6.4); main effect of object size $F(3,13) = 9.97$, $p < 0.001$. Response times were not assessed, because participants were asked to choose their answer from a randomly cycled array of possible answers, meaning that these measures would have been uninformative of task performance.

Insert Figure 5 about here.

Matrix 1. Results based on the first prediction matrix are illustrated in **Fig. 5**, and descriptions of significant clusters for this and the following analyses are reported in **Table 2**. Recall that this matrix captures regions for which activity patterns are more similar for objects of the same size, grasped with the same hand or seen on the same side, than for other size/laterality combinations. For the haptic task, the most prominent clusters in which this pattern is observed are bilateral and extend over the hand-related regions of the primary somatosensory and motor cortices. This finding shows that the brief and subtle movements required by our grasping task reliably engage the expected primary regions bilaterally. The visual task engaged bilateral occipital regions, again demonstrating the sensitivity of the procedure and participants' compliance with the instruction to maintain fixation. Note that due to the lack of full ventral coverage in some participants, the extent of ventral occipito-temporal activity is likely to be underestimated here.

Insert Figure 6 about here.

Matrix 2. Results of the second prediction matrix are illustrated in **Fig. 6**. This analysis identifies regions in which patterns of activity are increasingly similar to the extent that the grasped (or viewed) objects are similar in size. It tests this relationship only within conditions in which the same hand was used to execute the grasp (or the visual

stimulus appeared in the same hemifield). Note that unlike Matrix 1, here the cross-hand cells of the prediction matrix are empty (zero) meaning that similarities of patterns across the two hands (or two hemifields) contribute nothing to the searchlight results. In both tasks, this analysis reveals clusters of regions along the intraparietal sulcus, primarily in the left hemisphere, as well as prefrontal clusters predominantly in the haptic task.

Insert Figure 7 about here.

Matrix 3. The third prediction matrix (**Fig. 7**) complements the second one, in testing for regions in which the patterns of activity are more similar for more similar object sizes, only for conditions in which the objects were presented to different hands (or to different hemifields). Note broad similarity between regions identified here and in the orthogonal analysis of Matrix 2.

Insert Figure 8 about here.

Matrix 4. Results of the fourth prediction matrix are illustrated in **Fig. 8**. This matrix combines the two previous ones, so it is not independent of them. However, given that it incorporates the data in full (as opposed to only half in each of the preceding two analyses) we include it on the grounds that it should have better sensitivity to discover the predicted metrically size-sensitive regions. Accordingly, the results from the Matrix 4 analyses were used for a direct comparison between the haptic and visual sessions. While an informal comparison of their results suggests that distinct prefrontal and left intraparietal regions may be underpinning haptic (red/yellow) versus visual (blue/green) size-sensitive representations, a direct statistical comparison between the haptic and visual searchlight data did not reveal regions at corrected significance levels that were more reliably engaged by the haptic than the visual task.

Discussion

We used a combination of fMRI and searchlight MVPA to identify brain regions whose patterns of activity relate to the size of simple objects as perceived haptically. We described hypotheses about how size information may be encoded in a set of matrices that capture predictions about how similar the local patterns of brain activity should be in a given region, for objects of a given size relationship to each other.

The first such matrix described the prediction that grasps of a given object with a given hand would produce activity patterns that were consistently more reliable than different hand/size combinations. The brain regions identified in this analysis largely corresponded to primary motor and somatosensory cortices and were likely driven, in the main, by differences between using the left and right hands. This finding serves as a useful benchmark, demonstrating that the task and methods are sensitive to detect haptic activity, in spite of the subtle grasping movements involved. This analysis is also useful to distinguish the primary motor/somatosensory regions that are presumably involved in the peripheral, motoric aspects of performing the task, from those related to more abstract processes targeted by the subsequent analyses.

The aim of the remaining matrices was to identify such relatively abstract regions. Here we found lateral prefrontal and intraparietal regions that showed systematic sensitivity to object size, in the sense that more similar activity patterns were evoked by grasps of more similar object sizes. These patterns of results constitute evidence for metric size encoding both within-hand and across-hands that is distinct from the activity generated in primary motor/somatosensory regions. They are therefore consistent with the existence of a representation of haptic object size *per se*, independent of the specific afferents on which it is based, and independent of hand.

Our findings are consistent with three relevant strands of research that have tended to unfold independently. First, fMRI studies of haptic shape and orientation perception have found – with univariate analyses – activity in broadly similar regions (e.g. Kitada et al., 2006; Peltier et al., 2007; see also Sathian, 2016). For example, Peltier et al. (2007) identified several intraparietal and postcentral regions in a repetition-detection task by contrasting haptic exploration of smooth objects that varied in 3D shape, with uniformly shaped objects of different surface textures. Second, in studies of vision-for-action, a distinction is made (e.g. Hesse et al., 2016) between processing intrinsic (e.g. size) and

533 extrinsic (e.g. location) aspects of objects that are the target of manual actions.
534 Consistent with this distinction, Monaco et al. (2015) found a different set of regions that
535 displayed repetition suppression to objects of different sizes or locations - with anterior
536 intraparietal sulcus being implicated in visual assessment of size specifically.

537 Third, in studies of magnitude perception, an influential view holds that regions in and
538 around the intraparietal sulcus encode magnitude as expressed in numerosity, duration,
539 size, and other dimensions (Bueti and Walsh, 2009; Walsh, 2003). In response to this
540 proposal, in more recent work there has been a search for functional and anatomical
541 distinctions amongst the kinds of information these regions encode - again primarily in
542 the visual modality (e.g. Cohen-Kadosh et al., 2008; Pinel et al., 2004; see also
543 Hamamouche and Cordes, 2019). Notably, a recent study by Borghesani et al. (2019)
544 that sought to disentangle overlapping parietal responses evoked by number and length
545 of visual arrays, arrived independently at a multivoxel approach similar in logic to the
546 one applied here. That work revealed evidence for distinct, rather than shared, metric
547 representations of size and of number in the intraparietal region. With a similar aim,
548 Harvey et al. (2015) reported a high-resolution fMRI study revealing topographic cortical
549 maps of visual object size and numerosity in the superior parietal lobule. While these
550 maps overlap spatially, they also display distinct tuning and topology, suggesting
551 overlapping but functionally distinct encoding of these dimensions (cf. Peelen and
552 Downing, 2007). If the representation of haptic object size is similarly mapped over
553 regions of the intraparietal cortex, this could be one underlying contributor to the
554 success of the MVPA analyses in the present study.

555 In sum, then, our finding of metric size encoding with a haptic task, particularly in the
556 intraparietal region, is congruent not only with some previous studies of haptic
557 perception generally, but also with previous findings on visual size coding from studies
558 of action, and with findings related to magnitude estimation. In contrast, we did not find
559 evidence here for engagement of the secondary somatosensory cortex (SII), which may
560 have been anticipated on grounds of physiological evidence suggesting that neurons in
561 this region exhibit functional properties that would be useful for forming a representation
562 of size (e.g. relatively large, multi-finger receptive fields; sensitivity of receptive fields to
563 configuration of the digits; Fitzgerald et al., 2006a, b; Hsiao, 2008). It remains possible,
564 of course, that activity in the hand areas of SII is implicated in size estimation, but that it
565 is on a small enough spatial scale to be invisible to the multivoxel approach applied

here. It may also be possible that SII engagement would be more robust for whole-hand grasps, which pose a more complex integration problem relative to the precision grasp tested here.

Our participants also performed a visual size control task, with the aim of distinguishing haptic-specific representations from those relating to vision. Previous univariate fMRI work on discrimination of shape, texture, and orientation (e.g. Kitada et al., 2006; Peltier et al., 2007) took a similar approach and identified common regions of intraparietal activity across the two modalities for these kinds of tasks. Similarly, in the present study, whilst prefrontal and intraparietal regions engaged by haptic and visual tasks appeared distinct when compared informally in overlap maps, a direct statistical contrast did not identify subregions that were reliably engaged (in terms of multi-voxel patterns) more by one modality than by the other. Note that this direct comparison was hampered by reduced sensitivity (relative to the within-modality tests) given that the haptic and visual tasks were performed on separate days. Further, the spatial imprecision of the multivoxel searchlight approach imposes a limit on discriminating distinct but overlapping regions across contrasts. In that sense, our findings are not able to adjudicate clearly between shared and distinct visual and haptic object size representations. However, the methods developed here may prove suited to further efforts at detecting a dissociation, perhaps with higher spatial resolution (e.g. at higher field strengths; cf. Harvey et al., 2015).

If indeed there is distinct, modality-specific encoding of haptic size, what purpose might be served by such a representation? Within a hierarchical model of increasingly abstracted representations, it would reside between encoding at the level of sensory afferents and an integrated, amodal estimate of properties of the world. Raw sensory signals from the multiple haptic afferent systems could in principle feed directly into this ‘final’ integrated estimate, without the intermediate step of a haptic-specific representation. From a computational perspective, however, a haptic-specific step seems likely to be necessary. As outlined previously, haptic size constancy requires operations other than averaging or summation of different haptic signals (as per ‘optimal sensory integration’), but instead using signals to disambiguate one another: for example, using tactile signals about material properties to ‘compensate’ proprioceptive signals about hand opening (Berryman et al., 2006). This implies a distinct haptic-specific processing step.

599 Such a representation may also form a useful input to computations underlying visual-
600 haptic integration. Integrating across the senses yields performance improvements
601 because the brain exploits the statistical redundancy in multiple estimates of the same
602 property. To do this, the brain must know the statistics of the mapping between haptic
603 and visual signals, presumably acquired through long experience (Ernst, 2007). The
604 relationship between haptic object size and the raw sensory signals can change
605 substantially, however—consider wearing gloves, or using tools (Arbib et al., 2009;
606 Takahahshi and Watt, 2017)—in which case new mappings with vision would be
607 required for all the constituent haptic signals. In contrast, encoding haptic size
608 independent of the component afferent signals, and even the hand of origin, simplifies
609 sensory integration by allowing the same long-established statistical relationship to be
610 exploited in any situation.

611 In addition, of course, a haptic-specific estimate is useful in situations where integration
612 does not occur. Because we can (and routinely do) feel one object while looking at
613 another, sensory integration processes must determine when signals refer to the same
614 object, and should be integrated, and when they refer to different objects, in which case
615 an integrated result would be nonsensical, and signals should not be integrated (Ernst,
616 2007; Körding et al., 2007). In the latter situation the haptic-specific estimate must be
617 retained if the relevant perceptual property is to remain accessible. Consistent with this,
618 psychophysical evidence suggests that even when visual-haptic integration does occur,
619 the perceptual system retains access to the individual estimates from each sense (Hillis,
620 Ernst, Banks & Landy, 2002).

621 Taking these considerations together highlights a potential application of our approach,
622 to examine how haptic size estimates are encoded during the use of tools. Hand-held
623 tools (such as pliers) present interesting challenges to size perception in that 1) the
624 hands and the felt object are not spatially co-incident, as they would be in direct grasps;
625 and 2) some tools systematically magnify or minify the size of felt objects (depending on
626 the location of the fulcrum) and even – in the case of reverse pliers – invert the
627 relationship between grip aperture and grasp size. The similarity analysis developed
628 here could be applied to understanding the computations underlying tool use, for
629 example by distinguishing cortical regions whose activity patterns relate to the aperture
630 of the hand as opposed to the sensed size of a distal grasped object.

631 Finally, we turn to two specific aspects of our procedures and results that require further
632 comment. First, in spite of our extensive efforts to calibrate object sizes at the individual
633 participant level, based on psychophysical threshold estimation, we found in the
634 imaging experiment that performing the task on large object sizes (both visual and
635 haptic) was more difficult than for small object sizes. One contributing factor to this
636 result may be that the pre-scanning and scanning tasks were not identical: in the
637 psychophysical task, participants estimated which of two felt objects was the larger,
638 while in the scanner task participants performed a 4-alternative forced choice to
639 categorise the size of the object. Nonetheless, it is difficult to see how this main effect of
640 difficulty over object sizes should systematically distort similarities amongst the
641 underlying patterns of neural activity as observed here.

642 Second, the scanner size task tested here required participants to make an explicit size
643 judgment, and to do so categorically with reference to a learned set of four standard
644 sizes. A future study could apply the design logic of the present study to an implicit task
645 that has neither of these requirements. For example, participants could report on other
646 intrinsic (e.g. texture) or extrinsic (e.g. location) properties of each object, while size
647 varied incidentally and continuously. Compared with the present findings, this approach
648 would make it possible to distinguish haptic size representations that are task- and
649 context-invariant – “automatic” at least in some senses of the term -- from those that
650 reflect demands on the participant to overtly compare, categorize, and report an object’s
651 size. Separating implicit and continuous versus explicit and categorical haptic object
652 representations in this way could, in turn, provide a basis for better dissecting real-world
653 tasks that may rely to different degrees on such processes.

654

Acknowledgments

We are grateful to the Bangor Imaging Group for helpful ongoing discussions, to Andrew Fischer and Paul Mullins for MRI technical support, and to David McKiernan for developing the haptic size-discrimination apparatus.

Endnote

At the request of the authors, readers are herein alerted to the fact that additional materials related to this manuscript may be found in the Open Science Forum at https://osf.io/4t6u8/?view_only=3624ba70ef95474e920d2208a3bff060. (DOI: 10.17605/OSF.IO/4T6U8). These materials are not a part of this manuscript and have not undergone peer review by the American Physiological Society (APS). APS and the journal editors take no responsibility for these materials, for the website address, or for any links to or from it.

References

Arbib, M. A., Bonaiuto, J. B., Jacobs, S., Frey, S. H. (2009). Tool use and the distalization of the end-effector. Psychological Research, 73, 441–462.

Berryman, L. J., Yau, J. M., & Hsiao, S. S. (2006). Representation of object size in the somatosensory system. Journal of Neurophysiology, 96(1), 27-39.

Bodegård, A., Geyer, S., Grefkes, C., Zilles, K., & Roland, P. E. (2001). Hierarchical processing of tactile shape in the human brain. Neuron, 31(2), 317-328.

Borghesani, V., de Hevia, M. D., Viarouge, A., Pinheiro-Chagas, P., Eger, E., & Piazza, M. (2019). Processing number and length in the parietal cortex: Sharing resources, not a common code. Cortex, 114, 17-27.

Brainard, D. H. (1997). The psychophysics toolbox. Spatial vision, 10, 433-436.

Bruno, N., & Bertamini, M. (2010). Haptic perception after a change in hand size. Neuropsychologia, 48(6), 1853-1856.

Bueti, D., & Walsh, V. (2009). The parietal cortex and the representation of time, space, number and other magnitudes. Philosophical Transactions of the Royal Society of London B: Biological Sciences, 364(1525), 1831-1840.

Chouinard, P. A., Large, M. E., Chang, E. C., & Goodale, M. A. (2009). Dissociable neural mechanisms for determining the perceived heaviness of objects and the predicted weight of objects during lifting: An fMRI investigation of the size–weight illusion. Neuroimage, 44(1), 200-212.

Clark, J. J., Yuille, A. L. (1990). Data fusion for sensory information processing systems. Kluwer Academic Publishers, Boston.

Cohen Kadosh, R., Lammertyn, J., & Izard, V. (2008). Are numbers special? An overview of chronometric, neuroimaging, developmental and comparative studies of magnitude representation. Progress in neurobiology, 84(2), 132-147.

Coutanche, M. N., & Thompson-Schill, S. L. (2012). The advantage of brief fMRI acquisition runs for multi-voxel pattern detection across runs. *Neuroimage*, *61*(4), 1113-1119.

Deibert, E., Kraut, M., Kremen, S., & Hart, J. (1999). Neural pathways in tactile object recognition. Neurology, 52(7), 1413-1413.

Delhaye, B. P., Long, K. H., & Bensmaia, S. J. (2018). Neural Basis of Touch and Proprioception in Primate Cortex. Comprehensive Physiology, 8(4), 1575.

DiCarlo, J. J., Zoccolan, D., & Rust, N. C. (2012). How does the brain solve visual object recognition?. Neuron, 73(3), 415-434.

Edin, B. B., & Johansson, N. (1995). Skin strain patterns provide kinaesthetic information to the human central nervous system. The Journal of physiology, 487(1), 243-251.

Ernst, M. O. (2007). Learning to integrate arbitrary signals from vision and touch. Journal of Vision, 7, 1–14.

Ernst, M. O., & Banks, M. S. (2002). Humans integrate visual and haptic information in a statistically optimal fashion. Nature, 415, 429–433.

Etzel, J. A., Zacks, J. M., & Braver, T. S. (2013). Searchlight analysis: promise, pitfalls, and potential. Neuroimage, 78, 261-269.

Fabbri, S., Stubbs, K. M., Cusack, R., & Culham, J. C. (2016). Disentangling representations of object and grasp properties in the human brain. Journal of Neuroscience, 36(29), 7648-7662.

Fitzgerald, P. J., Lane, J. W., Thakur, P. H., & Hsiao, S. S. (2006a). Receptive field (RF) properties of the macaque second somatosensory cortex: RF size, shape, and somatotopic organization. Journal of Neuroscience, 26(24), 6485-6495.

Fitzgerald, P. J., Lane, J. W., Thakur, P. H., & Hsiao, S. S. (2006b). Receptive field properties of the macaque second somatosensory cortex: representation of orientation on different finger pads. Journal of Neuroscience, 26(24), 6473-6484.

Garrett, S., Barac-Cikoja, D., Carello, C., & Turvey, M. T. (1996). A parallel between visual and haptic perception of size at a distance. Ecological Psychology, 8(1), 25-42.

Gepshtein, S., & Banks, M. S. (2003). Viewing geometry determines how vision and haptics combine in size perception. Current Biology, 13, 483–488.

Ghahramani, Z., Wolpert, D. M., Jordan, M. I. (1997). Computational models of sensorimotor integration. In: Morasso PG, Sanguineti V (eds) Self-organization, computational maps, and motor control. Elsevier, Amsterdam, pp 117–147.

Hamamouche, K., & Cordes, S. (2019). Number, time, and space are not singularly represented: Evidence against a common magnitude system beyond early childhood. Psychonomic bulletin & review, 26(3), 833-854.

Harvey, B. M., Fracasso, A., Petridou, N., & Dumoulin, S. O. (2015). Topographic representations of object size and relationships with numerosity reveal generalized quantity processing in human parietal cortex. Proceedings of the National Academy of Sciences, 112(44), 13525-13530.

Haxby, J. V., Gobbini, M. I., Furey, M. L., Ishai, A., Schouten, J. L., & Pietrini, P. (2001). Distributed and overlapping representations of faces and objects in ventral temporal cortex. Science, 293(5539), 2425-2430.

Haynes, J. D., & Rees, G. (2006). Neuroimaging: decoding mental states from brain activity in humans. Nature Reviews Neuroscience, 7(7), 523.

765
766 Heed, T., Buchholz, V. N., Engel, A. K., & Röder, B. (2015). Tactile remapping: from
767 coordinate transformation to integration in sensorimotor processing. Trends in cognitive
768 sciences, 19(5), 251-258.
769
770 Hesse, C., Miller, L., & Buckingham, G. (2016). Visual information about object size and
771 object position are retained differently in the visual brain: Evidence from grasping
772 studies. Neuropsychologia, 91, 531-543.
773
774 Hillis, J. M., Ernst, M. O., Banks, M. S., & Landy, M. S. (2002). Combining Sensory
775 Information: Mandatory Fusion Within, but Not Between, Senses. Science, 298(5598),
776 1627-1630.
777
778 Hsiao, S. (2008). Central mechanisms of tactile shape perception. Current opinion in
779 neurobiology, 18(4), 418-424.
780
781 Jones, L. A., & Lederman, S. J. (2006). Human hand function. New York: Oxford
782 University Press.
783
784 Kim, S. S., Gomez-Ramirez, M., Thakur, P. H., & Hsiao, S. S. (2015). Multimodal
785 interactions between proprioceptive and cutaneous signals in primary somatosensory
786 cortex. Neuron, 86(2), 555-566.
787
788 Kitada, R., Kito, T., Saito, D. N., Kochiyama, T., Matsumura, M., Sadato, N., &
789 Lederman, S. J. (2006). Multisensory activation of the intraparietal area when
790 classifying grating orientation: a functional magnetic resonance imaging study. Journal
791 of Neuroscience, 26(28), 7491-7501.
792
793 Klatzky, R. L., Lederman, S. J., & Metzger, V. A. (1985). Identifying objects by touch: An
794 “expert system”. Perception & psychophysics, 37(4), 299-302.
795
796 Kleiner, M., Brainard, D., Pelli, D., Ingling, A., Murray, R., & Broussard, C. (2007).
797 What’s new in Psychtoolbox-3. Perception, 36(14).
798
799 Körding, K. P., Beierholm, U., Ma, W. J., Quartz, S., Tenenbaum, J. B., & Shams, L.
800 (2007). Causal inference in multisensory perception. PLoS ONE, 2, e943.
801
802 Kravitz, D. J., Saleem, K. S., Baker, C. I., Ungerleider, L. G., & Mishkin, M. (2013). The
803 ventral visual pathway: an expanded neural framework for the processing of object
804 quality. Trends in cognitive sciences, 17(1), 26-49.
805
806 Kriegeskorte, N., Goebel, R., & Bandettini, P. (2006). Information-based functional brain
807 mapping. Proceedings of the National Academy of Sciences, 103(10), 3863-3868.
808
809 Kriegeskorte, N., Mur, M., & Bandettini, P. A. (2008). Representational similarity
810 analysis-connecting the branches of systems neuroscience. Frontiers in systems
811 neuroscience, 2, 4.
812

Landy, M. S., Maloney, L. T., Johnston, E. B., Young, M. (1995). Measurement and modelling of depth cue combination: in defense of weak fusion. Vision Research, 35, 389–412.

Lederman, S., Gati, J., Servos, P., & Wilson, D. (2001). fMRI-derived cortical maps for haptic shape, texture, and hardness. Cognitive brain research, 12(2), 307-313.

Lederman, S. J., & Klatzky, R. L. (2009). Haptic perception: A tutorial. Attention, Perception, & Psychophysics, 71(7), 1439-1459.

Miquée, A., Xerri, C., Rainville, C., Anton, J. L., Nazarian, B., Roth, M., & Zennou-Azogui, Y. (2008). Neuronal substrates of haptic shape encoding and matching: a functional magnetic resonance imaging study. Neuroscience, 152(1), 29-39.

Monaco, S., Sedda, A., Cavina-Pratesi, C., & Culham, J. C. (2015). Neural correlates of object size and object location during grasping actions. European Journal of Neuroscience, 41(4), 454-465.

Moretto, G., & Di Pellegrino, G. (2008). Grasping numbers. Experimental Brain Research, 188(4), 505-515.

Norman, K. A., Polyn, S. M., Detre, G. J., & Haxby, J. V. (2006). Beyond mind-reading: multi-voxel pattern analysis of fMRI data. Trends in cognitive sciences, 10(9), 424-430.

O'Sullivan, B. T., Roland, P. E., & Kawashima, R. (1994). A PET study of somatosensory discrimination in man. Microgeometry versus macrogeometry. European Journal of Neuroscience, 6(1), 137-148.

Peelen, M. V., & Downing, P. E. (2007). Using multi-voxel pattern analysis of fMRI data to interpret overlapping functional activations. Trends in cognitive sciences, 11(1), 4-4.

Pelli, D. G. (1997). The VideoToolbox software for visual psychophysics: Transforming numbers into movies. Spatial vision, 10(4), 437-442.

Peltier, S., Stilla, R., Mariola, E., LaConte, S., Hu, X., & Sathian, K. (2007). Activity and effective connectivity of parietal and occipital cortical regions during haptic shape perception. Neuropsychologia, 45(3), 476-483.

Pinel, P., Piazza, M., Le Bihan, D., & Dehaene, S. (2004). Distributed and overlapping cerebral representations of number, size, and luminance during comparative judgments. Neuron, 41(6), 983-993.

Reed, C. L., Lederman, S. J., & Klatzky, R. L. (1990). Haptic integration of planar size with hardness, texture, and planar contour. Canadian Journal of Psychology/Revue canadienne de psychologie, 44(4), 522.

Reed, C. L., Shoham, S., & Halgren, E. (2004). Neural substrates of tactile object recognition: an fMRI study. Human brain mapping, 21(4), 236-246.

Sathian, K. (2016). Analysis of haptic information in the cerebral cortex. Journal of neurophysiology, 116(4), 1795-1806.

Savini, N., Babiloni, C., Brunetti, M., Caulo, M., Del Gratta, C., Perrucci, M. G., ... & Ferretti, A. (2010). Passive tactile recognition of geometrical shape in humans: an fMRI study. Brain research bulletin, 83(5), 223-231.

Simões-Franklin, C., Whitaker, T. A., & Newell, F. N. (2011). Active and passive touch differentially activate somatosensory cortex in texture perception. Human brain mapping, 32(7), 1067-1080.

Stoeckel, M. C., Weder, B., Binkofski, F., Buccino, G., Shah, N. J., & Seitz, R. J. (2003). A fronto-parietal circuit for tactile object discrimination:: an event-related fmri study. Neuroimage, 19(3), 1103-1114.

Stoesz, M. R., Zhang, M., Weisser, V. D., Prather, S. C., Mao, H., & Sathian, K. (2003). Neural networks active during tactile form perception: common and differential activity during macrospatial and microspatial tasks. International Journal of Psychophysiology, 50(1-2), 41-49.

Takahashi, C. & Watt, S.J. (2017). Optimal visual-haptic integration with articulated tools. Experimental Brain Research, 235, 1361-1373

Taylor, J. L. (2009). Proprioception. In L. R. Squire (Ed.), Encyclopedia of neuroscience (Vol. 7, pp. 1143-1149). Oxford: Academic Press.

Terada, K., Kumazaki, A., Miyata, D., & Ito, A. (2006). Haptic length display based on cutaneous-proprioceptive integration. Journal of Robotics and Mechatronics, 18(4), 489.

Walsh, V. (2003). A theory of magnitude: common cortical metrics of time, space and quantity. Trends in cognitive sciences, 7(11), 483-488.

Yau, J. M., Kim, S. S., Thakur, P. H., & Bensmaia, S. J. (2015). Feeling form: the neural basis of haptic shape perception. Journal of neurophysiology, 115(2), 631-642.

898 **Figure Captions**
899
900 **Figure 1.** Out-of-scanner haptic size-discrimination experiment. a**)** Computer-controlled
901 device for presenting different-sized 'objects'. **b)** Participant during testing, showing
902 occluding screen. **c)** Schematic procedure of the out-of-scanner behavioural task. **d)**
903 Psychometric function fits for one example participant at the five object sizes, for
904 objects grasped with the left hand. Red, cyan, blue, green and purple symbols/curves
905 denote 10, 20, 30, 40 and 50 mm standard object sizes, respectively. The diameter of
906 the data symbols is proportional to the number of trials at each comparison size. **e)**
907 Just-noticeable differences in haptic size as a function of standard size, for the data
908 shown in panel d. The coloured crosses denote the JNDs for each size. The black curve
909 is a second-order polynomial fit to the JNDs. The orange, numbered circles show the
910 four candidate object sizes for the fMRI experiment derived from these data, spaced 2
911 JNDs apart, and centred around 30 mm (see main text).

912 **Figure 2.** Top. Apparatus for the haptic fMRI task. Participants grasped unseen wooden
913 blocks of different sizes arranged on a sliding tray. The apparatus lay on a plastic table
914 that straddled the participant's body; it was completely out of the participant's field of
915 view. An experimenter was in the scanner room with the participant, and followed cues
916 to slide the mechanism into the correct position for each trial. As described in the main
917 text (and see Fig 1), the sizes of the four blocks were selected on a participant-by-
918 participant basis, according to the results of the initial behavioural experiment. Bottom.
919 Schematic of the trial sequence in the haptic/visual fMRI experiments. A text cue
920 indicated whether to grasp with the left or right hand (haptic task) or whether an object
921 would appear on the left or right side of the screen (visual task). An auditory cue then
922 signalled the instruction to grasp (haptic task) or view (visual task) the object. Objects
923 were of one of four sizes, for which participants learned the labels A-D. The letters "A",
924 "B", "C", and "D" were presented on screen, cycled in a random order. Participants
925 selected the letter corresponding to their size judgment by pressing a foot pedal.

926 **Figure 3.** Similarity matrices expressing different predictions about how patterns of
927 brain activity might systematically relate to object size. Main image: over a given pair of
928 scanning runs, for a given participant, for a given brain region, we can measure the
929 similarity of the patterns of brain activity for every combination of hand (left, right) with
930 object size (1-4). Different matrices express different predictions about what form this

similarity structure should take. Matrix 1 (in the main panel) expresses that the voxelwise pattern of activity for a given hand x size combination will be more similar across runs than for any different combination. Matrices 2 and 3 (side panels, top and middle) express the prediction that more similar object sizes (e.g. size 2 and 3) will evoke more similar activity patterns than more dissimilar sizes (e.g. size 1 and 4). In Matrix 2 this is tested for the within-hand case and in Matrix 3 for the cross-hand case. Matrix 4 (side panel, bottom) is the combination of Matrices 2 and 3, and tests for similarities in patterns of activity based on object size but irrespective of the effector used. The actual matrix weights used in the analyses are reported numerically in Table 1. The schematic checkerboards depicting prediction matrices also appear below in the figures that present related results.

Figure 4. Schematic illustration of the analysis approach. Each participant performed 8 runs of the haptic task. For each unique pair of runs (28 pairs), searchlight analyses were conducted over the entire cortex. At each searchlight location (not shown to scale), the similarity of the neural patterns evoked by each hand x object size combination was measured with a correlation. The resulting 8x8 similarity matrix was multiplied element-wise by a normalised predicted similarity matrix (Table 1) that captured a predicted pattern of activity (Figure 3), and this product averaged to compute a single scalar result value. To the extent that activity in given searchlight position was similar to the predicted pattern, this would generate a relatively high result value. Each of these values populated a results map at the centre of each searchlight sphere. The resulting 28 searchlight maps were Fisher transformed at each voxel, before being averaged and then spatially smoothed. The resulting maps formed the basis for a second-level random-effects analysis across participants. These procedures were performed separately for data from the haptic and visual tasks.

Figure 5. Results of the whole-brain searchlight analysis, testing the match at each searchlight location to the similarity pattern captured in Matrix 1 (shown at bottom right). This analysis tests for regions in which the voxelwise pattern of activity for a given hand x size combination (haptic task) or side x size (visual task) is more similar across runs than for any different combination. The value over each slice refers to its Z plane in MNI space. The scale bar indexes the T value at each voxel location from a group-wise random effects analysis of searchlight results. Results from the haptic task are shown in warm colours and from the visual task in cool colours. Overlapping significant voxels

964 are depicted in purple. Note that the figures depict separate analyses of the two tasks
965 and do not represent a direct statistical comparison between them. The statistical
966 overlays are thresholded at $p<0.001$ voxelwise, $p<0.05$ cluster-wise, with no cluster
967 extent threshold. The underlying anatomical image is the average of the normalised
968 structural T1 images from all 16 participants. The left side of each slice corresponds to
969 the left hemisphere of the brain. See also **Table 2**.

970 **Figure 6.** Results of the whole-brain searchlight analysis related to Matrix 2. This tests
971 for regions in which more similar object sizes (e.g. 2 and 3) evoke more similar activity
972 patterns than more dissimilar sizes (e.g. 1 and 4), for grasps with the same hand (or for
973 objects shown at the same visual location). Conventions as in **Fig. 5**.

974 **Figure 7**. Results of the whole-brain searchlight analysis related to Matrix 3. This tests
975 for regions in which more similar object sizes (e.g. 2 and 3) evoke more similar activity
976 patterns than more dissimilar sizes (e.g. 1 and 4), for grasps with different hands (or for
977 objects shown at different visual locations). Conventions as in **Fig. 5**.

978 **Figure 8**. Results of the whole-brain searchlight analysis related to Matrix 4. This tests
979 for regions in which more similar object sizes evoke more similar activity patterns than
980 more dissimilar sizes, both within and across hands (or both within and across visual
981 locations). Conventions as in **Fig. 5**.

982

983 **Table 1.** Similarity matrix weights. These matrices enumerate the numerical weights
984 that were used to conduct the whole-brain searchlight pattern analyses of pattern
985 similarity. They are illustrated graphically in Figure 3.

	Similarity matrix weights							
	0.875	-0.125	-0.125	-0.125	-0.125	-0.125	-0.125	-0.125
	-0.125	0.875	-0.125	-0.125	-0.125	-0.125	-0.125	-0.125
	-0.125	-0.125	0.875	-0.125	-0.125	-0.125	-0.125	-0.125
	-0.125	-0.125	-0.125	0.875	-0.125	-0.125	-0.125	-0.125
	-0.125	-0.125	-0.125	-0.125	0.875	-0.125	-0.125	-0.125
	-0.125	-0.125	-0.125	-0.125	-0.125	0.875	-0.125	-0.125
	-0.125	-0.125	-0.125	-0.125	-0.125	-0.125	0.875	-0.125
Matrix 1	-0.125	-0.125	-0.125	-0.125	-0.125	-0.125	-0.125	0.875
	1.25	0.25	-0.75	-1.75	0	0	0	0
	0.25	1.25	0.25	-0.75	0	0	0	0
	-0.75	0.25	1.25	0.25	0	0	0	0
	-1.75	-0.75	0.25	1.25	0	0	0	0
	0	0	0	0	1.25	0.25	-0.75	-1.75
	0	0	0	0	0.25	1.25	0.25	-0.75
	0	0	0	0	-0.75	0.25	1.25	0.25
Matrix 2	0	0	0	0	-1.75	-0.75	0.25	1.25
	0	0	0	0	1.25	0.25	-0.75	-1.75
	0	0	0	0	0.25	1.25	0.25	-0.75
	0	0	0	0	-0.75	0.25	1.25	0.25
	0	0	0	0	-1.75	-0.75	0.25	1.25
	1.25	0.25	-0.75	-1.75	0	0	0	0
	0.25	1.25	0.25	-0.75	0	0	0	0
	-0.75	0.25	1.25	0.25	0	0	0	0
Matrix 3	-1.75	-0.75	0.25	1.25	0	0	0	0
	1.25	0.25	-0.75	-1.75	1.25	0.25	-0.75	-1.75
	0.25	1.25	0.25	-0.75	0.25	1.25	0.25	-0.75
	-0.75	0.25	1.25	0.25	-0.75	0.25	1.25	0.25
	-1.75	-0.75	0.25	1.25	-1.75	-0.75	0.25	1.25
	1.25	0.25	-0.75	-1.75	1.25	0.25	-0.75	-1.75
	0.25	1.25	0.25	-0.75	0.25	1.25	0.25	-0.75
	-0.75	0.25	1.25	0.25	-0.75	0.25	1.25	0.25
Matrix 4	-1.75	-0.75	0.25	1.25	-1.75	-0.75	0.25	1.25

986

987

988 **Table 2**. Significant family-wise error corrected clusters for the random-effects analyses
989 reported in Figures 5-8. Brain region labels are indicative. The first four major rows
990 relate to the haptic size task, and the following four rows to the visual size task.

Contrast	Brain Region	Volume mm^3	MNI coordinates			F value	p FWE-corr (cluster level)
			x	y	z		
Haptic matrix 1 	R precentral gyrus	502	30	-34	47	39.19	<.001
	L precentral gyrus	401	-27	-20	65	36.17	<.001
	R Supplementary motor cortex	68	6	-12	59	31.51	<.001
	R precentral gyrus	61	8	-27	53	30.12	.001
Haptic matrix 2 	R superior frontal gyrus	69	18	18	53	47.56	.001
	L supramarginal gyrus	39	-54	-40	44	25.04	.023
	R precuneus	41	6	-57	26	38.47	.018
	L middle frontal gyrus	101	-37	20	41	32.76	<.001
	L superior parietal lobe	37	-32	-54	44	30.55	.029
	R superior/middle frontal gyrus	65	20	28	38	30.42	.001
	R supramarginal gyrus	46	48	-44	50	28.03	.010
Haptic matrix 3 	R superior frontal gyrus	84	16	20	53	65.76	<.001
	R precuneus	41	3	-47	44	50.55	.015
	L middle frontal gyrus	218	-37	23	38	51.65	<.001
	L superior parietal lobe	139	-32	-54	47	42.25	<.001
	R superior/middle frontal gyrus	70	28	23	38	43.37	.001
	R supramarginal gyrus	130	46	-40	41	56.42	<.001
	L angular gyrus	40	-42	-64	26	33.15	.017
	R angular gyrus	52	43	-60	23	31.10	.004
Haptic matrix 4 	R superior frontal gyrus	71	16	18	53	73.24	.003
	R precuneus	42	3	-47	44	49.92	.031
	L middle frontal gyrus	139	-37	20	38	44.57	<.001
	L superior parietal lobe	118	32	-54	44	39.56	<.001
	R middle frontal gyrus	64	28	23	38	39.62	.005
	R supramarginal gyrus	65	46	-40	41	45.90	.004

991
992

993

Contrast	Brain Region	Volume mm3	MNI coordinates			F value	p FEW-corr (cluster level)
			x	y	z		
Visual matrix 1 	R precuneus	26	18	-60	29	36.54	.040
Visual matrix 2 	L middle frontal gyrus	40	-30	50	11	68.37	.016
	L superior parietal lobe	198	-24	-44	44	43.72	<.001
	L middle frontal gyrus	71	-42	33	29	43.45	<.001
	L supramarginal gyrus	32	-52	-40	47	28.46	.045
	L supplementary motor cortex	47	-4	13	44	27.64	.007
Visual matrix 3 	L superior parietal lobe	257	-37	-42	44	41.08	<.001
	R occipital gyrus	66	28	-74	35	48.86	.001
	L angular gyrus	23	-44	-60	20	32.14	.007
	L superior frontal gyrus	32	-7	58	8	29.47	.040
Visual matrix 4 	L middle frontal gyrus	58	-30	53	11	92.47	.012
	L superior parietal lobe	203	-34	-44	44	45.59	<.001
	L middle frontal gyrus	41	-42	33	29	30.51	.049
	L Supplementary motor cortex	41	-2	13	44	26.54	.049

994

995

996

997

998

999

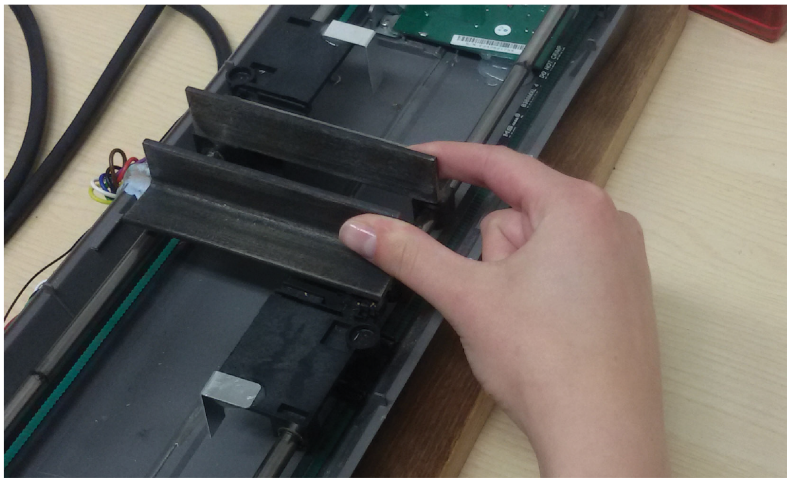

a.

b.

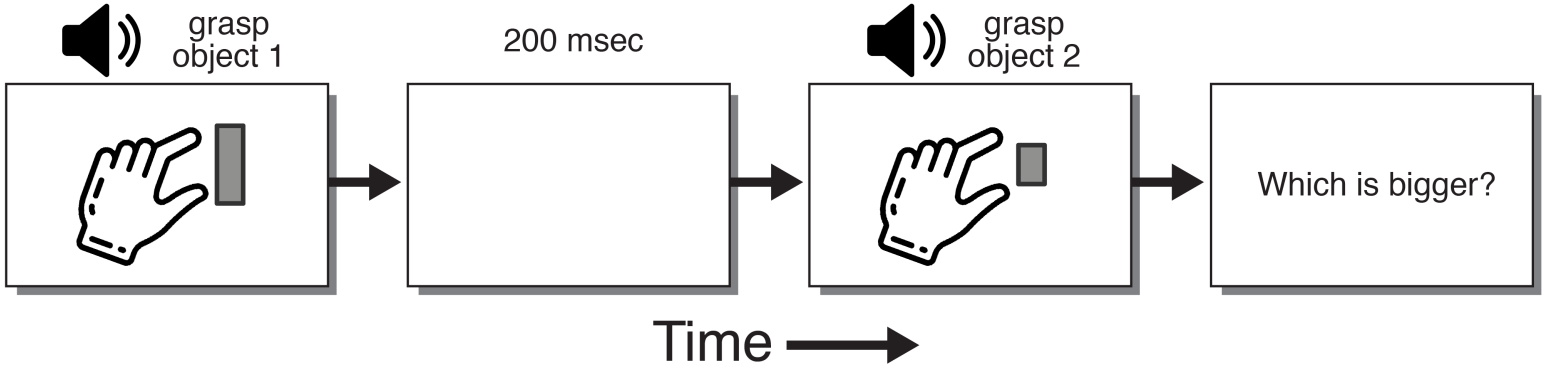
grasp
object 1
200 msec
grasp
object 2
Which is bigger?
Time

c.

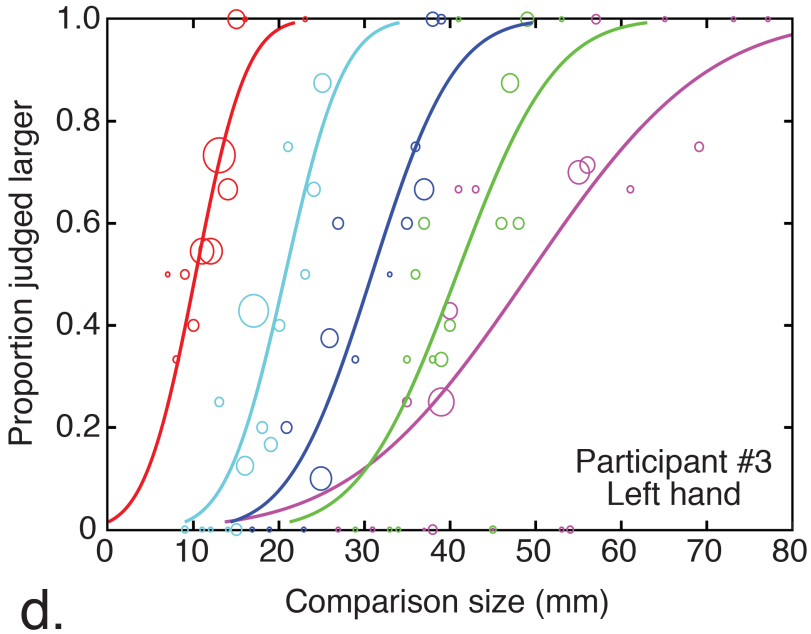
Proportion judged larger
1.0
0.8
0.6
0.4
0.2
0
0
10
20
30
40
50
60
70
80
Participant #3
Left hand
Comparison size (mm)

d.

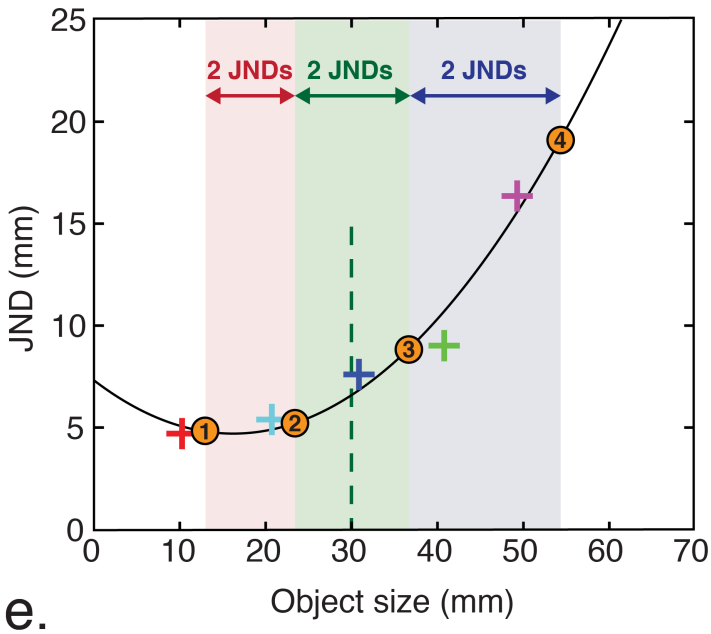
2 JNDs
2 JNDs
2 JNDs
JND (mm)
25
20
15
10
5
0
0
10
20
30
40
50
60
70
1
2
3
4
Object size (mm)

e.

a)

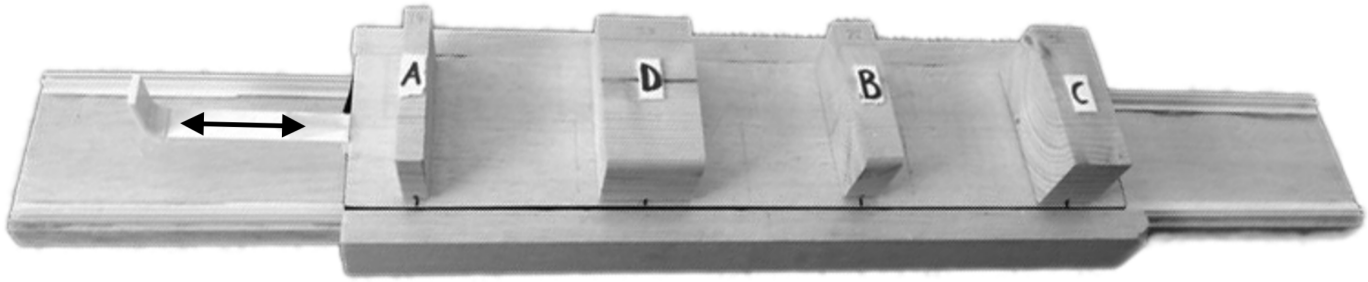
A
D
B
C

b)

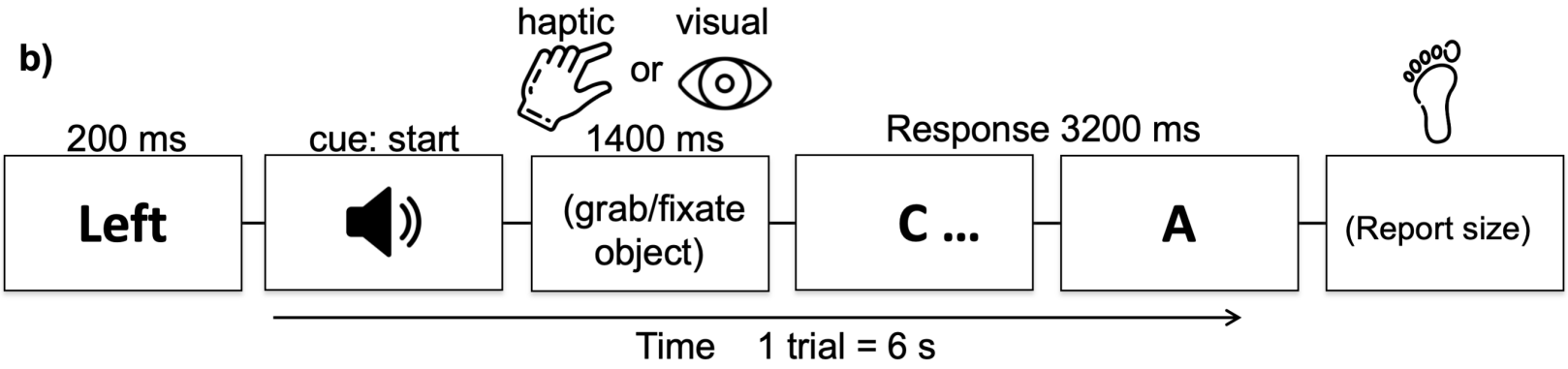
haptic
visual
or
200 ms
cue: start
1400 ms
Response 3200 ms
Left
(grab/fixate object)
C ...
A
(Report size)
Time
1 trial = 6 s

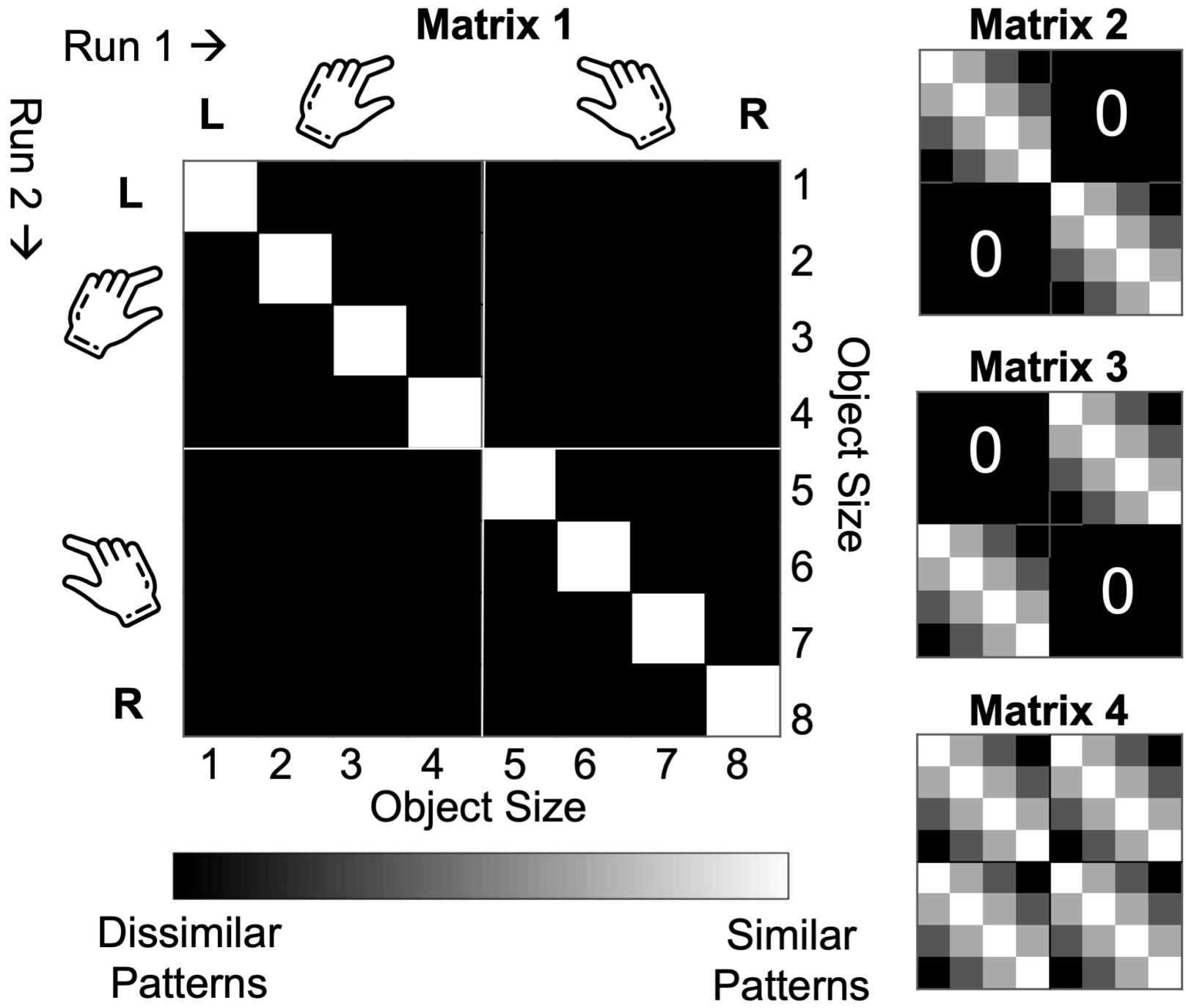
Matrix 1
Run 1 →
Run 2 →
L
R
L
R
1
2
3
4
5
6
7
8
Object Size
1 2 3 4 5 6 7 8
Object Size
Dissimilar Patterns
Similar Patterns
Matrix 2
0
0
Matrix 3
0
0
Matrix 4

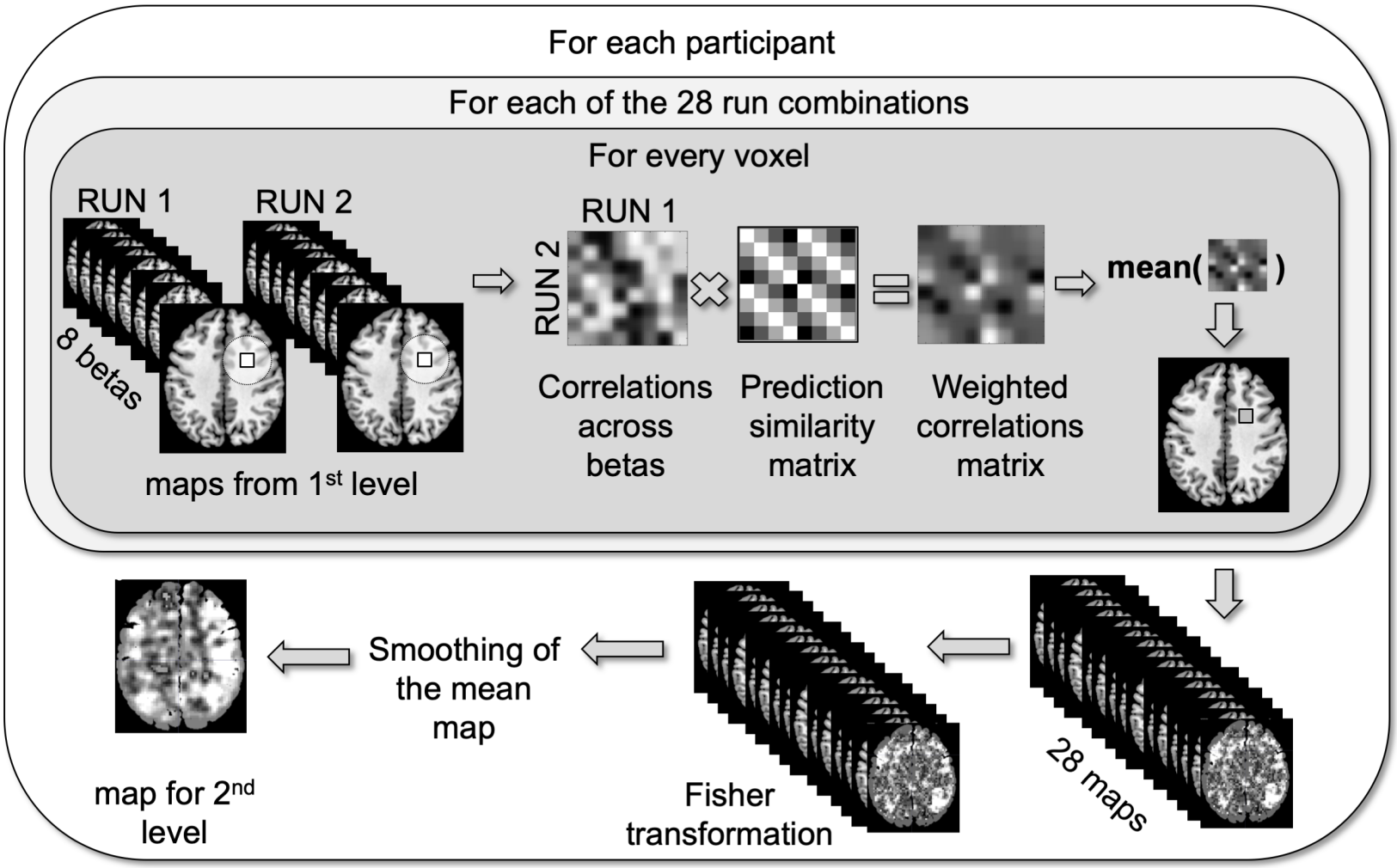
For each participant
For each of the 28 run combinations
For every voxel
RUN 1
RUN 2
8 betas
maps from 1st level
RUN 1
RUN 2
Correlations across betas
Prediction similarity matrix
Weighted correlations matrix
mean( )
28 maps
Fisher transformation
Smoothing of the mean map
map for 2nd level

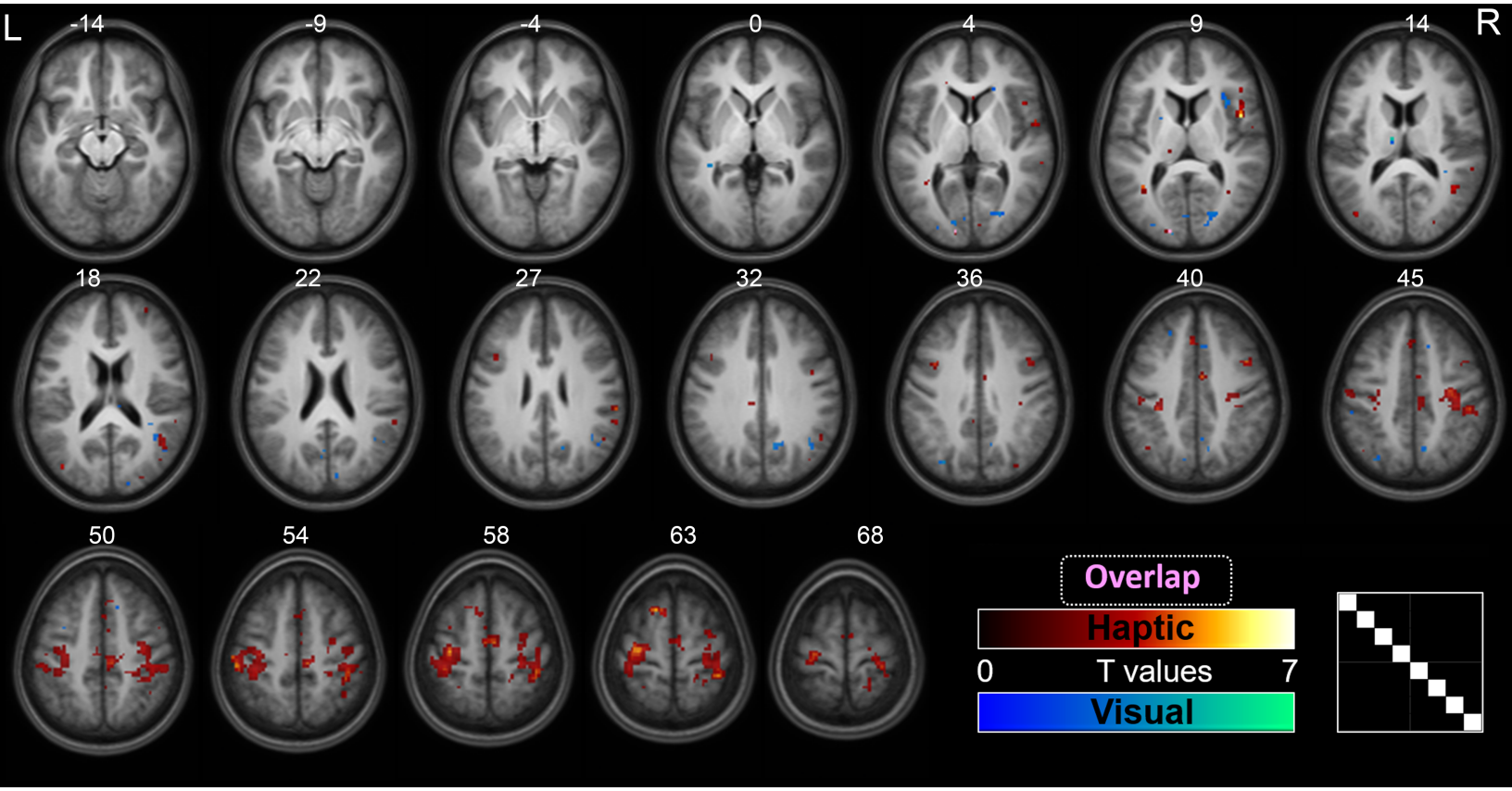
L
R
-14
-9
-4
0
4
9
14
18
22
27
32
36
40
45
50
54
58
63
68
Overlap
Haptic
0
T values
7
Visual

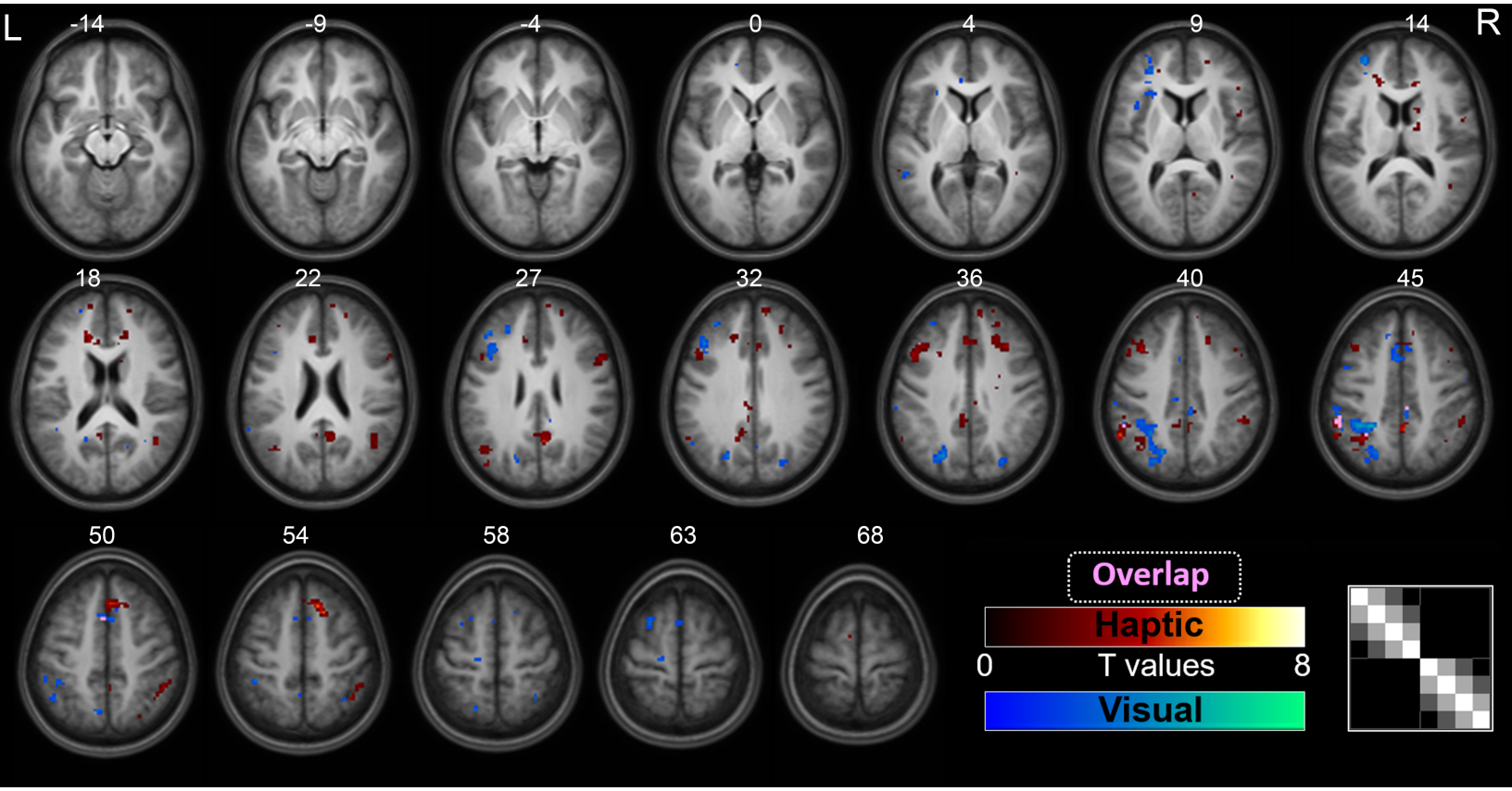
L
R
-14
-9
-4
0
4
9
14
18
22
27
32
36
40
45
50
54
58
63
68
Overlap
Haptic
0
T values
8
Visual

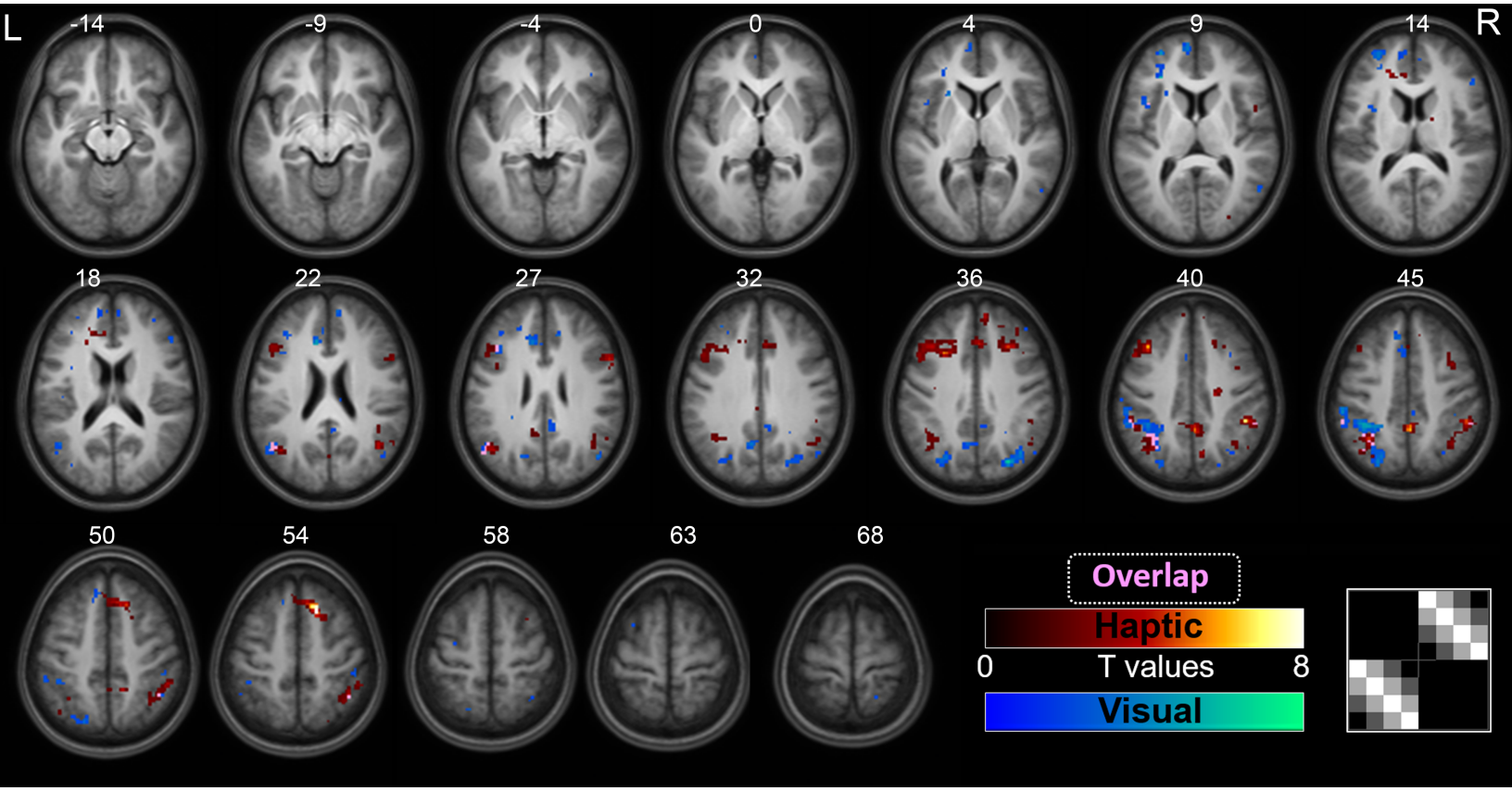
L
R
-14
-9
-4
0
4
9
14
18
22
27
32
36
40
45
50
54
58
63
68
Overlap
Haptic
0
T values
8
Visual

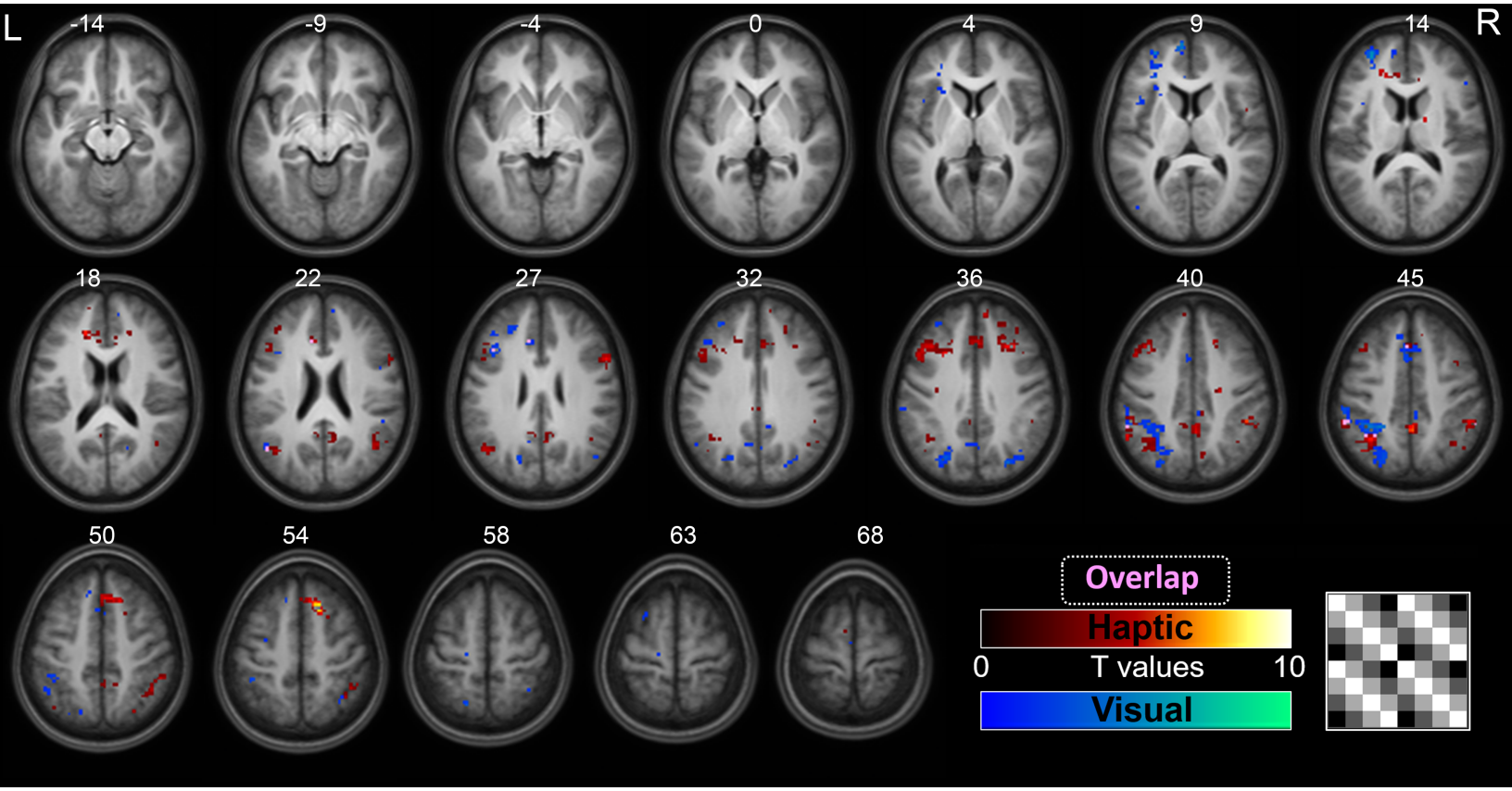
L
R
-14
-9
-4
0
4
9
14
18
22
27
32
36
40
45
50
54
58
63
68
Overlap
Haptic
0
T values
10
Visual

Table 1. Similarity matrix weights. These matrices enumerate the numerical weights that were used to conduct the whole-brain searchlight pattern analyses of pattern similarity. They are illustrated graphically in Figure 3.

	Similarity matrix weights							
	0.875	-0.125	-0.125	-0.125	-0.125	-0.125	-0.125	-0.125
	-0.125	0.875	-0.125	-0.125	-0.125	-0.125	-0.125	-0.125
	-0.125	-0.125	0.875	-0.125	-0.125	-0.125	-0.125	-0.125
	-0.125	-0.125	-0.125	0.875	-0.125	-0.125	-0.125	-0.125
	-0.125	-0.125	-0.125	-0.125	0.875	-0.125	-0.125	-0.125
	-0.125	-0.125	-0.125	-0.125	-0.125	0.875	-0.125	-0.125
	-0.125	-0.125	-0.125	-0.125	-0.125	-0.125	0.875	-0.125
Matrix 1	-0.125	-0.125	-0.125	-0.125	-0.125	-0.125	-0.125	0.875
	1.25	0.25	-0.75	-1.75	0	0	0	0
	0.25	1.25	0.25	-0.75	0	0	0	0
	-0.75	0.25	1.25	0.25	0	0	0	0
	-1.75	-0.75	0.25	1.25	0	0	0	0
	0	0	0	0	1.25	0.25	-0.75	-1.75
	0	0	0	0	0.25	1.25	0.25	-0.75
	0	0	0	0	-0.75	0.25	1.25	0.25
Matrix 2	0	0	0	0	-1.75	-0.75	0.25	1.25
	0	0	0	0	1.25	0.25	-0.75	-1.75
	0	0	0	0	0.25	1.25	0.25	-0.75
	0	0	0	0	-0.75	0.25	1.25	0.25
	0	0	0	0	-1.75	-0.75	0.25	1.25
	1.25	0.25	-0.75	-1.75	0	0	0	0
	0.25	1.25	0.25	-0.75	0	0	0	0
	-0.75	0.25	1.25	0.25	0	0	0	0
Matrix 3	-1.75	-0.75	0.25	1.25	0	0	0	0
	1.25	0.25	-0.75	-1.75	1.25	0.25	-0.75	-1.75
	0.25	1.25	0.25	-0.75	0.25	1.25	0.25	-0.75
	-0.75	0.25	1.25	0.25	-0.75	0.25	1.25	0.25
	-1.75	-0.75	0.25	1.25	-1.75	-0.75	0.25	1.25
	1.25	0.25	-0.75	-1.75	1.25	0.25	-0.75	-1.75
	0.25	1.25	0.25	-0.75	0.25	1.25	0.25	-0.75
	-0.75	0.25	1.25	0.25	-0.75	0.25	1.25	0.25
Matrix 4	-1.75	-0.75	0.25	1.25	-1.75	-0.75	0.25	1.25

Table 2. Significant family-wise error corrected clusters for the random-effects analyses reported in Figures 5-8. Brain region labels are indicative. The first four major rows relate to the haptic size task, and the following four rows to the visual size task.

Contrast	Brain Region	Volume mm^3	MNI coordinates			F value	p FWE-corr (cluster level)
			x	y	z		
Haptic matrix 1 	R precentral gyrus	502	30	-34	47	39.19	<.001
	L precentral gyrus	401	-27	-20	65	36.17	<.001
	R Supplementary motor cortex	68	6	-12	59	31.51	<.001
	R precentral gyrus	61	8	-27	53	30.12	.001
Haptic matrix 2 	R superior frontal gyrus	69	18	18	53	47.56	.001
	L supramarginal gyrus	39	-54	-40	44	25.04	.023
	R precuneus	41	6	-57	26	38.47	.018
	L middle frontal gyrus	101	-37	20	41	32.76	<.001
	L superior parietal lobe	37	-32	-54	44	30.55	.029
	R superior/middle frontal gyrus	65	20	28	38	30.42	.001
	R supramarginal gyrus	46	48	-44	50	28.03	.010
Haptic matrix 3 	R superior frontal gyrus	84	16	20	53	65.76	<.001
	R precuneus	41	3	-47	44	50.55	.015
	L middle frontal gyrus	218	-37	23	38	51.65	<.001
	L superior parietal lobe	139	-32	-54	47	42.25	<.001
	R superior/middle frontal gyrus	70	28	23	38	43.37	.001
	R supramarginal gyrus	130	46	-40	41	56.42	<.001
	L angular gyrus	40	-42	-64	26	33.15	.017
	R angular gyrus	52	43	-60	23	31.10	.004
Haptic matrix 4 	R superior frontal gyrus	71	16	18	53	73.24	.003
	R precuneus	42	3	-47	44	49.92	.031
	L middle frontal gyrus	139	-37	20	38	44.57	<.001
	L superior parietal lobe	118	32	-54	44	39.56	<.001
	R middle frontal gyrus	64	28	23	38	39.62	.005
	R supramarginal gyrus	65	46	-40	41	45.90	.004

Contrast	Brain Region	Volume mm3	MNI coordinates			F value	p FEW-corr (cluster level)
			x	y	z		
Visual matrix 1 	R precuneus	26	18	-60	29	36.54	.040
Visual matrix 2 	L middle frontal gyrus	40	-30	50	11	68.37	.016
	L superior parietal lobe	198	-24	-44	44	43.72	<.001
	L middle frontal gyrus	71	-42	33	29	43.45	<.001
	L supramarginal gyrus	32	-52	-40	47	28.46	.045
	L supplementary motor cortex	47	-4	13	44	27.64	.007
Visual matrix 3 	L superior parietal lobe	257	-37	-42	44	41.08	<.001
	R occipital gyrus	66	28	-74	35	48.86	.001
	L angular gyrus	23	-44	-60	20	32.14	.007
	L superior frontal gyrus	32	-7	58	8	29.47	.040
Visual matrix 4 	L middle frontal gyrus	58	-30	53	11	92.47	.012
	L superior parietal lobe	203	-34	-44	44	45.59	<.001
	L middle frontal gyrus	41	-42	33	29	30.51	.049
	L Supplementary motor cortex	41	-2	13	44	26.54	.049